Final Report

DEPARTMENT OF THE NAVY
OFFICE OF THE CHIEF OF NAVAL RESEARCH
APPLIED HYDRODYNAMICS RESEARCH PROGRAM

For Work Completed Under Grant
ONRN00014-91-J-1086

NUMERICAL SIMULATION OF PARTICLE-WAVE INTERACTION ON BOUNDARY LAYERS

Principal Investigator: Dr. Sedat Biringen
Professor
Department of Aerospace Engineering Sciences
University of Colorado
Boulder, Colorado 80309
(303)-492-4760

Graduate Student: E. M. Saiki

Summary

This research program involves a computational study of the effects of disturbances generated from a moving particle on boundary layer transition. The practical importance of this problem stems from the fact that as an underwater vehicle moves through a particulate environment, particles enter the boundary layer and produce local disturbances. These disturbances may act as a bypass mechanism to transition and turbulence by interacting with boundary layer instabilities. The objective of this research is to study the basic mechanisms of the particle interaction and its effect on transition in the boundary layer. For this purpose, a direct numerical simulation is undertaken and the spherical particle is represented by a forcing function in the Navier Stokes equations. Results reveal good agreement with experimental studies. The report is presented in two parts. The first part concerns a general overview of the work accomplished and the second part summarizes our recent efforts on the modeling of steady/unsteady flow over a cylinder.

Technical Approach :

The full, three-dimensional, time-dependent Navier Stokes equations are integrated on a nonstaggered mesh by a time splitting method which implements the implicit Crank-Nicolson scheme on the normal diffusion terms and the Adams-Bashforth method on the remaining terms. Fourth-order central finite differences are applied in the streamwise direction and the spectral Chebyshev matrix method is employed along the wall-normal direction. The spanwise direction is assumed periodic enabling the use of Fourier expansions. The procedure allows for nonperiodic inflow/outflow boundary conditions so that a realistic spatially-evolving simulation can be obtained. The pressure Poisson equation is solved by the capacitance matrix method and staggered grids were used in the normal direction.

To simulate the boundary of the sphere in the flow within a Cartesian geometry, we implement a technique developed by Peskin (1982) and further explored by Goldstein, Handler, and Sirovich (1993). This technique involves the imposition of a no-slip boundary in a flow through a feedback forcing function which is added to the momentum equations. The feedback function effectively brings the fluid velocity to zero at the desired points in the flow which define the no-slip boundary.

Summary of Work Accomplished

Experimental studies (Blackwelder, Browand, Fisher, and Tanaguichi 1992) using moving particles with a diameter of roughly $\frac{1}{3}$ the boundary layer thickness have observed the development of turbulent spots due to the effect of a particle wake in the boundary layer. The wake of the particle was found to travel downstream developing essentially streamwise vortices which then formed a turbulent spot. In an effort to model this scenario the following tasks have been undertaken.

1. A numerical simulation of the spatial evolution of an isolated disturbance in boundary layer flow in order to test the capability of the code to capture an event such as a turbulent spot.
2. The body of the particle itself was introduced into the boundary layer through a no-slip boundary technique.
3. An investigation of the effect of a stationary spherical particle on boundary layer transition.

Significance of These Accomplishments

In this section, we summarize and highlight the main points of the research accomplished during the past year.

Isolated disturbance

This computation involved the prescription of a pair of counter rotating streamwise vortices as initial conditions. During the course of these simulations, we found good agreement in the development of the disturbance in comparison with the temporal simulations of Breuer and Landahl (1990). In particular, we obtained what Breuer and Landahl (1990)

describe as a secondary instability developing in the center of the disturbance which is dominated by high two-dimensional modes. This behavior in our results and those of Breuer and Landahl (1990) was most noticeable in contours of normal velocity in the centerline x-y plane shown in Fig. 1a. We repeated these calculations using a higher mesh resolution and determined that the secondary instability was in actuality a numerical instability caused by insufficient resolution in the normal direction. The results shown in Fig. 1b reveal that the secondary instability does not appear, i.e. the main positive cell of normal velocity upstream does not split into two cells, in agreement with the temporal simulations of Henningson, Lundbladh, and Johansson (1993).

Figure 2 presents the time evolution of the localized disturbance through contours of perturbation streamwise velocity contours in a x-z plane at $y \approx 1.05$ for the higher normal resolution case. The initial disturbance forms a wedge-like shape as spanwise gradients are formed by high speed streaks surrounding the low speed core of fluid at the centerline. Similar development was observed in both Breuer and Landahl (1990) and Henningson *et al.* (1993).

Flow over a cylinder

In this next section we demonstrate the use of the forcing function method in several test cases. Figure 3 details the time evolution of the streamfunction and spanwise vorticity contours of uniform flow over a cylinder. The vorticity contours reflect the step-like definition of the boundary of the cylinder with some small upstream effects however, the downstream development of the flow is smooth. As observed by Bouard and Coutanceau (1980), a "bulge" of fluid appears half way between the top of the cylinder and the stagnation point, which forms a secondary eddy (Fig. 3b) whose direction of rotation is opposite that of the main eddy.

The second test case we consider involves a stationary cylinder in boundary layer flow. A sequence of "snapshots" of streamfunction contours detailing the evolution of the flow around the cylinder in time is presented in Fig. 4. In the initial stages, the behavior of the fluid as it passes above the cylinder is similar to that which occurs when a cylinder is placed in uniform flow. Two vortices are shed from the top of the cylinder which break off and are convected downstream. After this transient stage, a steady state is reached and a recirculation zone appears behind the cylinder. Due to the presence of the wall, a large bubble of reverse flow develops behind the cylinder; its length at steady state is ≈ 55 nondimensional units behind the cylinder. This final state is qualitatively in agreement with experimental observations (Bearman and Zdravdovich, 1978).

Flow over a sphere

Next, we applied the external force technique to the simulation of a sphere in boundary layer flow. In these computations, a stationary sphere was placed in the boundary layer at a fixed height and the development of the wake of the sphere was investigated and compared with experimental observations. Two cases with low and high Reynolds numbers of $Re_{\delta_0^*} = 500$ and 750, respectively, are considered. The particle Reynolds numbers for the two cases are $Re_d = 322$ and $Re_d = 494$ for the low and high Reynolds cases, respectively. Here, Re_d is defined as $Re_d = \frac{ud}{\nu}$, where d is the diameter of the sphere, ν is kinematic

viscosity, and, if y_d denotes the height of the top of the sphere above the wall, u is the velocity of the undisturbed boundary layer flow at y_d. An even higher Reynolds number case ($Re_{\delta^*} = 950$, $Re_d = 645$) was examined, however, as observed in the experiments a turbulent wedge began to form and we were unable to continue the computation due to insufficient grid resolution.

Figure 5 presents streamwise vorticity isosurfaces for the low Reynolds number case. The pattern appearing in these figures is similar to the hairpin vortex shedding stage in the flow visualization experiments of Vincent and Petrie, (1993). Positive and negative streamwise vorticity regions form "legs" which lift upward towards the freestream. Further downstream from the sphere, these vortices are convected away as their strength decays. This can be observed in a clearer manner in Fig. 6 which shows a x-z cross-section of streamwise vorticity contours at the top of the sphere near $y = 1.3$. Vortex pairs are shed in the wake of the sphere; the Strouhal frequency of this shedding is $\approx .2$ in good agreement with experimental measurements. The value of Re_d for this case falls below $(Re_d)_{crit}$ found in the results of Hall (1967) and Vincent and Petrie (1993), thus no turbulent wedge should appear.

In the high Reynolds number case the value of $Re_d = 494$ lies near $(Re_d)_{crit}$ as determined by Hall (1967), therefore a turbulent wedge within the wake may form. Vincent and Petrie (1993) observed the breakdown of the flow into a turbulent wedge through a series of stages, beginning first with the appearance of hairpin vortices. The heads of the vortices rise, while their legs descend and then attach to the wall. Accompanying the initiation of the hairpin vortices is the appearance of a thin layer of fluctuating fluid near the wall which ultimately breaks down into a turbulent wedge. The initial stages of this scenario are shown in Figs. 7 and 8. In Fig. 7, isosurfaces of streamwise vorticity suggest the development of the hairpin vortices. Here, as in the lower Reynolds number case, the heads of the vortices rise however, in accordance with Vincent and Petrie (1993), the legs are beginning to descend towards the wall. Below the vortices a thin strip of streamwise vorticity forms. Figure 8 demonstrates the organization of the the vortices within the wake of the sphere through streamwise vorticity contours in the x-z plane near the top of the sphere. In this calculation we found that a larger spanwise length in the computational domain is needed to capture the full development of the wake. A computation employing a spanwise length of 4π is currently in progress.

List of Publications :

Refereed Journal Publications :

1. Saiki, E. M., Biringen, S., Danabasoglu, G., and Streett, C. L., 1993. "Spatial simulation of secondary instability in channel flow: comparison of K- and H-type disturbances," *J. Fluid Mech.*, **253**, 495.
2. Danabasoglu, G., Biringen, S., and Streett, C. L. "Application of the spectral multidomain method to the Navier-Stokes equations," to appear in *J. Comp. Physics*.
3. Huser, A. and Biringen, S., 1993. "Numerical simulation of turbulent flow in a square duct," *J. Fluid Mech.*, **257**, 65.

4. Huser, A. and Biringen, S. "Direct numerical simulation of turbulent flow in a square duct: Reynolds stress and dissipation rate budgets," *Phys. Fluids.* (in press)
5. Biringen, S., Saiki, E. M., Danabasoglu, G., and Streett, C. L. "Spatial simulation of transition in plane channel flow: effects of random initial conditions," to be submitted to *Phys. Fluids.*

Refereed Symposium Proceedings :

1. Danabasoglu, G., Biringen, S. and Streett, C. L., 1993. "Simulation of instabilities in a boundary layer with a roughness element," in *13th Int. Conf. Num. Meth. in Fluid Dyn.*, (Eds. M. Napolitano and F. Sabetta), Springer-Verlag, 205.
2. Danabasoglu, G., Biringen, S., and Streett, C. L., 1993. "Spatial simulation of boundary layer instability: effects of surface roughness," AIAA 93-0075.
3. Huser, A. and Biringen, S., 1993. "Direct numerical simulation of turbulent flow in a square duct," AIAA 93-0198.
4. Saiki, E. M. and Biringen, S., 1994. "Numerical simulation of spherical particle effects on boundary layer flow," to appear in *NASA/ICASE Transition, Turbulence, and Combustion Proceedings*, Springer-Verlag.

Abstracts and Technical Reports

1. Danabasoglu, G., Biringen, S., and Streett, C. L., 1992. "Simulation of boundary layer instability in the presence of a roughness element," *Bull. Amer. Phys. Soc.*, **37**, 1812.
2. Reichert, R. S., Hatay, F. F., and Biringen, S., 1992. "Proper orthogonal decomposition (POD) with two inhomogenous directions," *Bull. Amer. Phys. Soc.*, **37**, 1775.
3. Huser, A. and Biringen, S., 1992. "Simulation of turbulent flow in a square duct: Reynolds stress and dissipation budget rates." *Bull. Amer. Phys. Soc.*, **37**, 1715.
4. Saiki, E. M. and Biringen, S., 1993. "Effect of a spherical particle on boundary layer transition," Paper to be presented at the 46th Ann. Meeting DFD/APS, Albuquerque. New Mexico, Nov. 21-23.

References :

Bearman, P. W. and Zdravdovich, M. M., 1978. "Flow around a cylinder near a plane boundary," *J. Fluid Mech.* **89**, 33.

Blackwelder, R. F., Browand, F. K., Fisher, C., and Tanaguichi, P., 1992. "Initiation of turbulent spots in a laminar boundary layer by rigid particulates," *Bull. Am. Phys. Soc.* **37**, 1812.

Bouard R. and Coutanceau, M., 1980. "The early stage of development of the wake behind an impulsively started cylinder for $40 < Re < 10^4$," *J. Fluid Mech.*, **101**, 583.

Breuer, K. S. and Landahl, M. T., 1990. "The evolution of a localized disturbance in a laminar boundary layer, Part 2. Strong disturbances," *J. Fluid Mech.*, **220**, 595.

Goldstein, D., Handler, R., and Sirovich, L., 1993. "Modeling a no-slip flow boundary with an external force field," *J. Comp. Physics*, **105**, 354.

Hall, G. R., 1967. "Interaction of the wake from bluff bodies with an initially laminar boundary layer," *AIAA J.*, **5**, 1386.

Henningson, D. S., Lundbladh, A., and Johansson, A., 1993. "A mechanism for bypass transition from localized disturbances in wall-bounded shear flows," *J. Fluid Mech.*, **250**, 169.

Peskin, C. S., 1982." The fluid dynamics of heart valves: experimental, theoretical, and computational methods," *Ann. Rev. Fluid Mech.*, 14, 235.

Vincent, D. C. and Petrie, H. L., 1993. "Transition induced by a spherical particle in a laminar boundary layer," AIAA 93-2909.

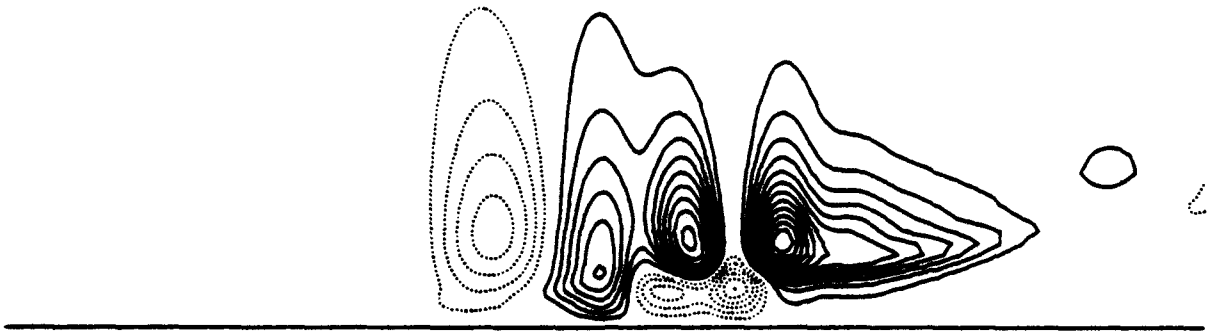

(a)

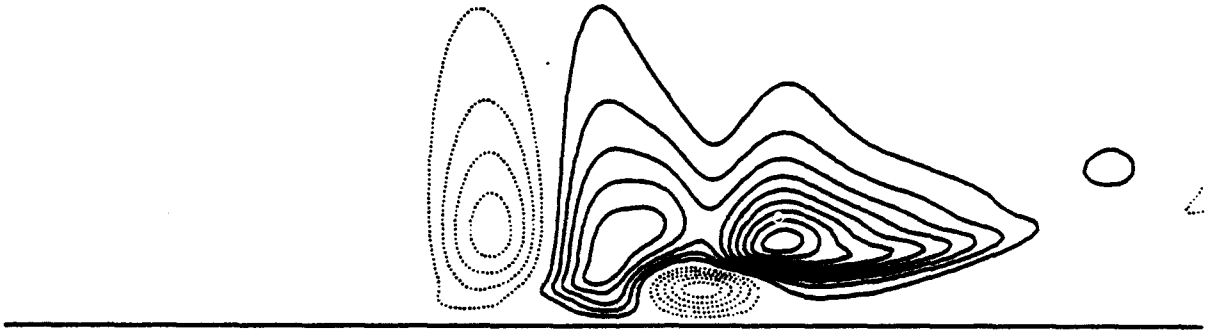

(b)

Figure 1. Contours of normal perturbation velocity in the x-y plane at $z = 25$. t=163.6: (a) $380 \times 71 \times 33$: (b) $380 \times 101 \times 33$. The contour interval is 0.0005. Note the disappearance of secondary instability in the high resolution case (b).

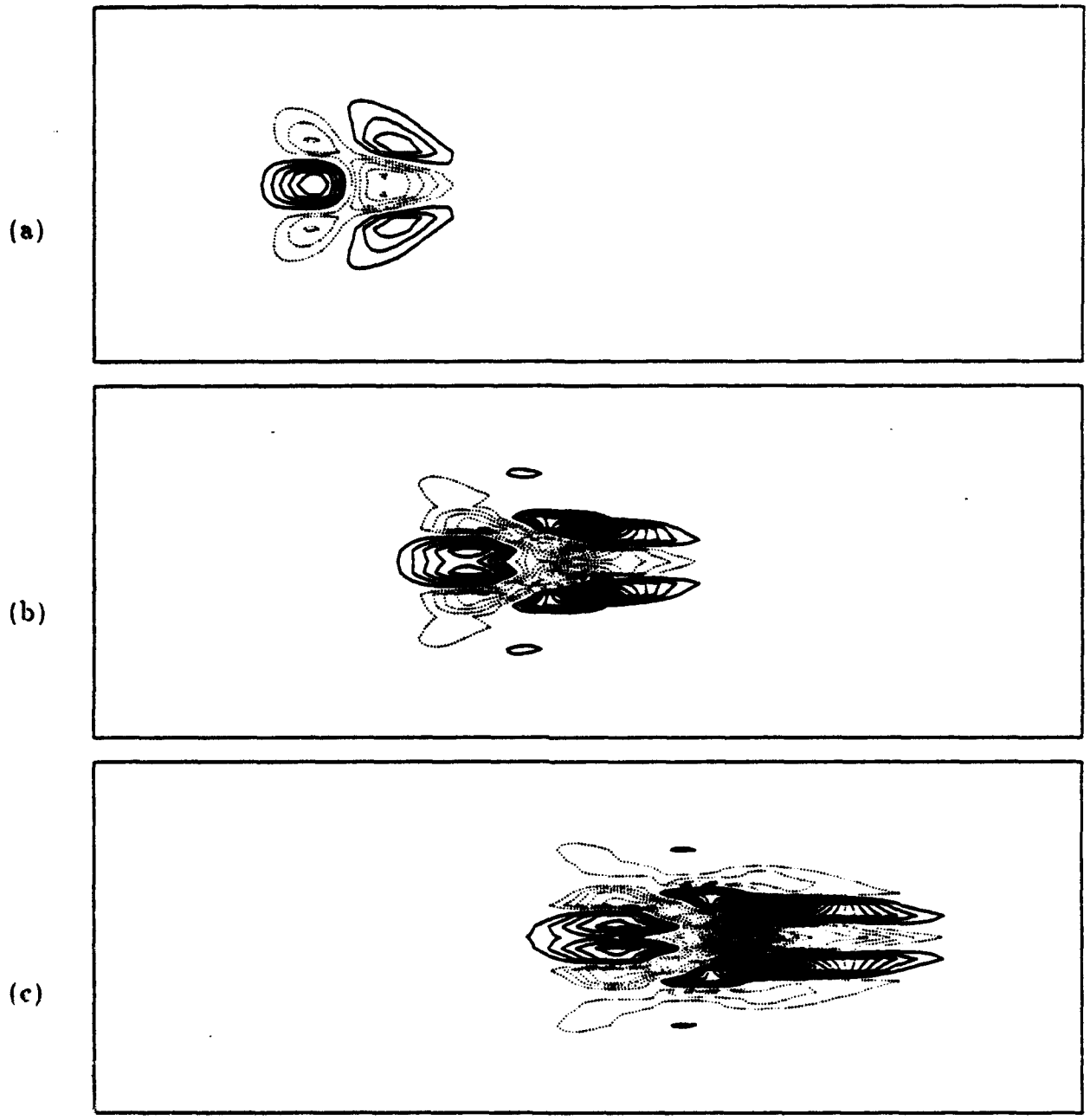

Figure 2. Time evolution of perturbation streamwise velocity contours in the x-z plane near $y \approx 1.05$: (a) $t = 85.08$: (b) $t = 137.4$: (c) $t = 189.9$. The contour interval is 0.01. The streamwise vortices elongate along x and intensify to form spot-like structures.

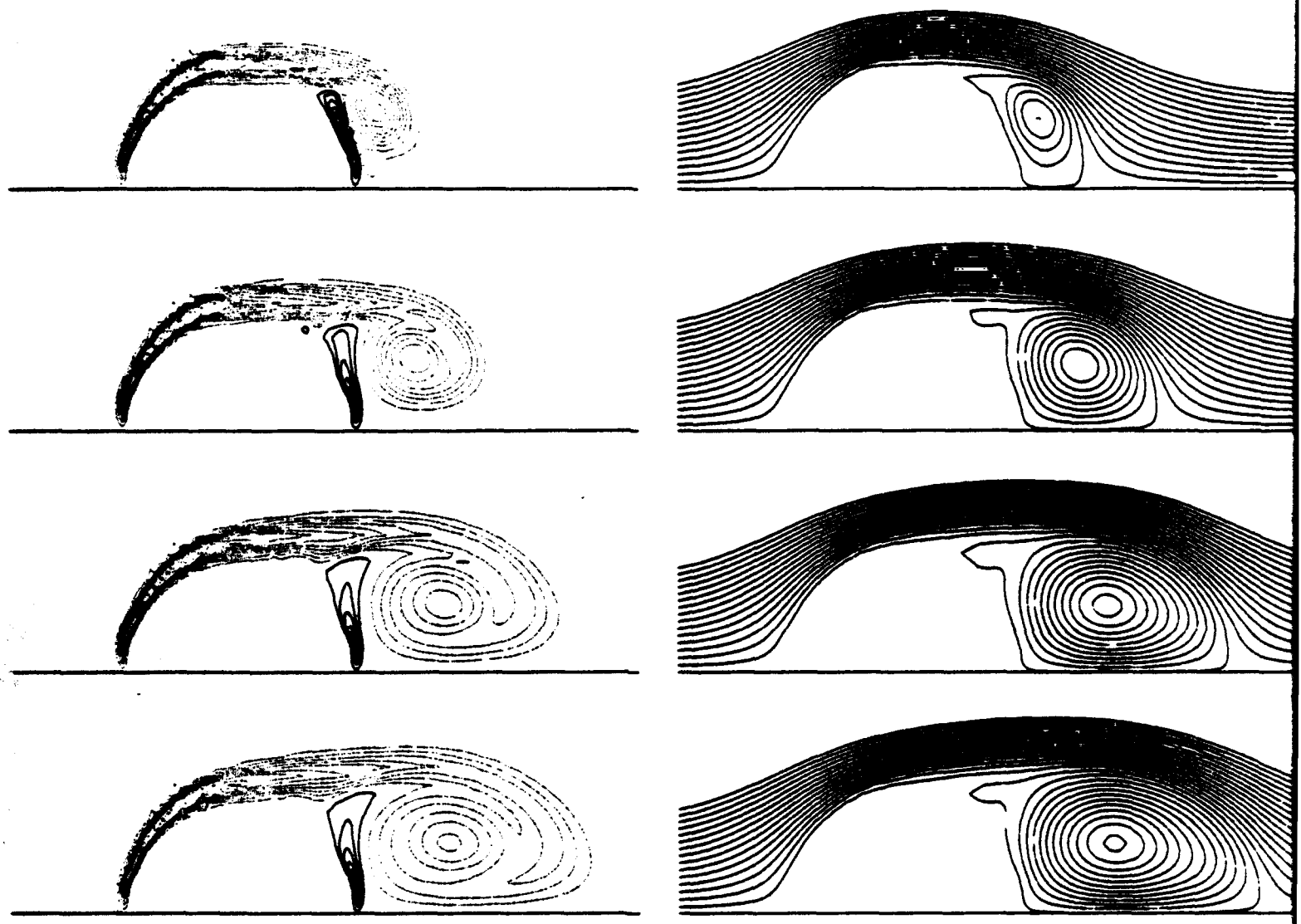

(a) (b)

Figure 3. Startup flow over a cylinder for t = 1.00. 1.75. 2.50. 3: Re=550: (a) spanwise vorticity: (b) streamfunction. These contours reveal the formation of a counter rotating secondary vortex half way between the top of the cylinder and the stagnation point.

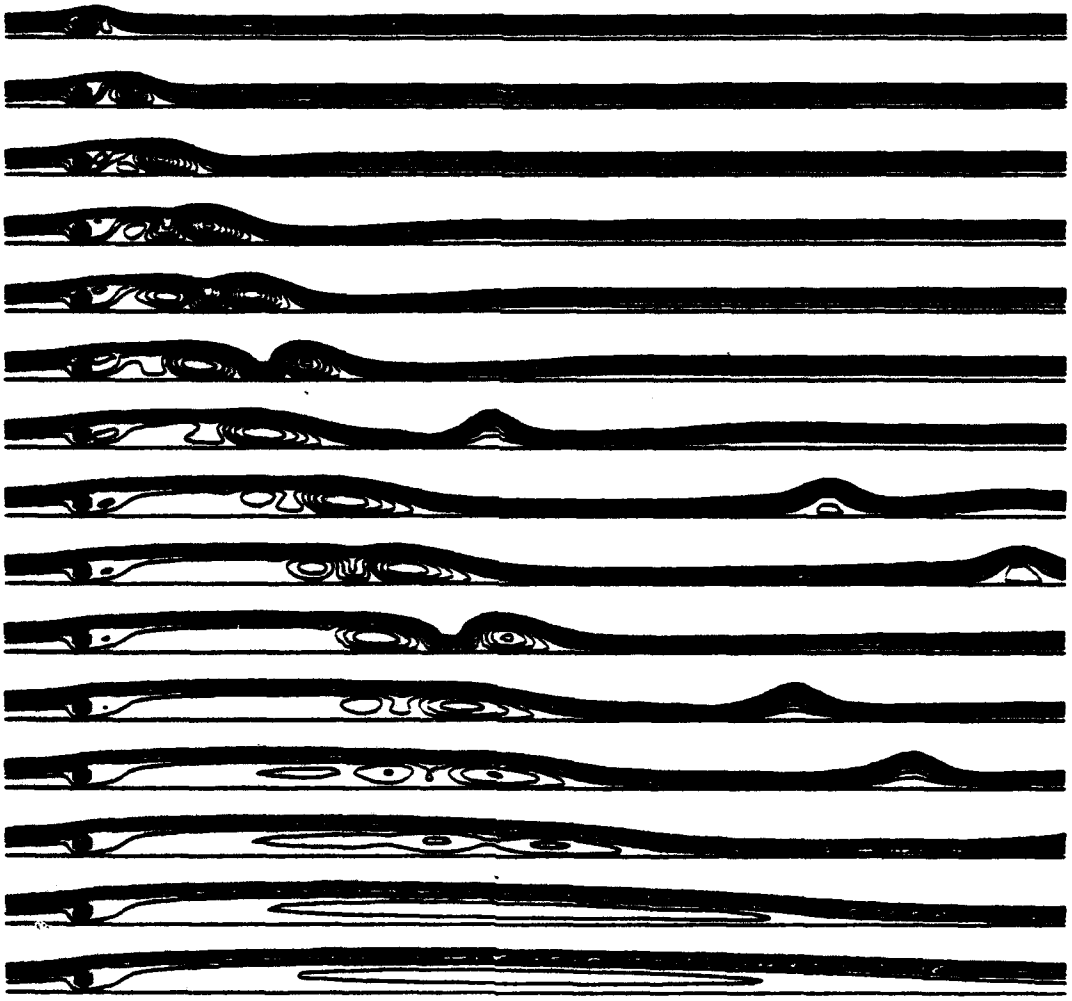

Figure 4. Evolution of the flow over a cylinder in the boundary layer. Each time frame corresponds to t = 3. 8. 16. 29. 37. 46. 64. 91. 109. 127. 154. 163. 181. 271. and 1019 nondimensional time units. After two vortices are shed and convected downstream, a large separation bubble develops at steady state.

Figure 5. Isosurfaces (level=±.1) of streamwise vorticity for flow past a sphere in boundary layer flow: $Re_{\delta_0^*} = 450$. $Re_d = 322$. The streamwise extent shown is $x \approx 25$-58.5 nondimensional lengths. Vortex "legs" lift upwards towards the freestream. resembling the vortex shedding stage observed in experiments.

Figure 6. Contours of streamwise vorticity in the x-z plane at $y = 1.3$ for flow past a sphere in boundary layer flow: $Re_{\delta_0^*} = 450$. $Re_d = 322$. The streamwise extent shown is $x \approx 25$-64 nondimensional lengths. The contour interval is 0.05. Vortex pairs are shed in the wake which decay as they move away from the sphere.

Figure 7. Isosurfaces (level=±.2) of streamwise vorticity for flow past a sphere in boundary layer flow: $Re_{\delta_0^*} = 750$. $Re_d = 494$. The streamwise extent shown is $x \approx 25$-66 nondimensional lengths. Vortex "legs" lift towards the freestream and begin to descend towards the wall.

Figure 8. Contours of streamwise vorticity in the x-z plane at $y = 1.3$ for flow past a sphere in boundary layer flow: $Re_{\delta_0^*} = 750$. $Re_d = 494$. The streamwise extent shown is $x \approx 25$-66 nondimensional lengths. The contour interval is 0.1. In the inital stages, organized vortex pairs develop in the wake of the sphere.

NUMERICAL SIMULATION OF A CYLINDER IN UNIFORM FLOW: APPLICATION OF A VIRTUAL BOUNDARY METHOD

E. M. Saiki and S. Biringen

Department of Aerospace Engineering Sciences

Uni ersity of Colorado

Abstract

In this study, a virtual boundary technique is applied to the numerical simulation of stati nary and moving cylinders in uniform flow. This approach readily allows the imposition of a no-slip boundary within the flow field by a feedback forcing term added to the momentum equations. In the present work, this technique is used with a high-order finite difference method effectively eliminating spurious oscillations caused by the feedback forcing when used with spectrally discretized flow solvers. Very good agreement is found between the present calculations and previous computational and experimental results for steady and time dependent flow at low Reynolds numbers.

Introduction

The fundamental fluid dynamics problem of a circular cylinder in uniform flow has been examined extensively in both computational and experimental studies and is considered a stringent test for flow solvers. The difficulty which accompanies the computational approach to this problem by finite differences or spectral methods lies in the representation of the cylinder geometry to allow for an accurate application of these numerical integration methods. The use of coordinate transformations and mapping techniques is possible, but requires a highly accurate way of calculating the transformation Jacobians. Finite element methods (Gresho, Chan, Upson, & Lee 1984; Engelman & Jaminia 1990; Karniadakis & Triantafyllou 1992) and conformal transformations (Jordan & Fromm 1972; Braza, Chassaing, & Minh 1986; Badr & Dennis 1985) have been used with success for this problem. As an alternative to the use of generalized coordinates and coordinate transformations for finite difference and spectral methods, Peskin (1972) developed a method which represents a body within a flow field via a forcing term added to the governing equations. When applied at certain points in the flow, this forcing term simulates the effect of the body on the flow allowing for the modeling of a no-slip boundary of any shape within a Cartesian computational box without the necessity of mapping. Peskin (1972, 1982) successfully implemented this method in modeling moving boundaries in heart valve simulations. Peskin's method (immersed boundary technique) requires an implicit solution scheme to determine the forcing term and it is partially dependent upon the material properties, *e.g.* stiffness and thickness of the heart muscle, and on internal forces which maintain the definition of the boundary of the body as it moves through the flow field. Using a similar approach, Goldstein, Handler, & Sirovich (1993) developed a simpler virtual boundary method, which employs a forcing term governed by a feedback loop. Unlike the approach conceived by Peskin (1972, 1982), this scheme does not rely on an implicit solution algorithm to determine the forcing term. Goldstein et al. (1993) have applied this procedure to an investigation on the effects of riblets on turbulent channel flow using a spectral method. They noted that the forcing function generated constant low amplitude, high frequency oscillations which they were able to control by numerical low-pass filters. Their turbulent flow simulations were not noticeably affected by these spurious signals,

but such numerical oscillations may become of concern when one calculates the evolution of a forced disturbance wave as in the simulation of flow instability and transition.

In the present study, we use the method developed by Goldstein *et al.* (1993) to simulate stationary, rotating, and oscillating cylinders in uniform flow at low Reynolds numbers ($Re \leq 400$) allowing the assessment of the virtual boundary technique to model a body in an unsteady flow field. In the present solution procedure, high-order finite differences are implemented in order to suppress the numerical oscillations caused by the forcing function observed in the Chebyshev spectral method of Goldstein *et al.* (1993).

Computational Method

The numerical model integrates the two-dimensional, time-dependent, incompressible, Navier-Stokes and continuity equations nondimensionalized by the diameter of the cylinder, D, and the free-stream velocity, U_∞, on a staggered mesh by a time splitting method. The normal diffusion terms are advanced implicitly by the Crank-Nicolson scheme and an explicit third-order compact Runge Kutta method is applied to the remaining terms (Streett & Hussaini 1986). The equations are discretized spatially in the normal (y) and streamwise (x) directions by fourth-order central finite differences. The pressure Poisson equation is evaluated by the tensor product method (Huser & Biringen 1992).

At the upper and lower boundaries, we impose shear free conditions, *i.e.* $\frac{\partial u}{\partial y} = 0$ and $v = 0$ and at the inflow boundary, uniform flow conditions are assumed, *i.e.* $u = 1$ and $v = 0$. At the outflow, boundary conditions are prescribed to ensure that wave-like disturbances (generated by the vortex shedding) in the high Reynolds number cases leave the computational domain without reflection. This was accomplished by appending a "buffer domain" to the physical domain (the length of the buffer domain was about 20-30% of the physical domain) in which the governing equations were modified by reducing the streamwise viscous terms and the right hand side of the pressure Poisson equation to zero at the outflow boundary using a smooth coefficient function. Previous numerical experiments have included rigorous testing of this technique verifying its suitability for use in both high and low amplitude wave propagation problems (Streett & Macaraeg 1989;

Danabasoglu, Biringen, & Streett 1991; Danabasoglu 1992; Saiki, Biringen, Danabasoglu, & Streett 1993).

In implementing the method of Goldstein *et al.* (1993) to the present calculations of flow over a cylinder, the no-slip boundary of the cylinder surface was represented by a feedback forcing function added to the momentum equations. This feedback function effectively brings the fluid velocity to zero at the desired points in the flow which define the no-slip boundary and can be expressed as

$$\mathbf{F}(\mathbf{x}_s,t) = \alpha \int_0^t (\mathbf{U}(\mathbf{x}_s,t) - \mathbf{v}(\mathbf{x}_s,t))dt + \beta(\mathbf{U}(\mathbf{x}_s,t) - \mathbf{v}(\mathbf{x}_s,t)). \tag{1}$$

Here, $\mathbf{F}$ is the external force imposed at the discrete surface points defined by $\mathbf{x}_s$, and $\mathbf{U}$ is the fluid velocity at these surface points. The velocity of the body itself is controlled by specifying $\mathbf{v} = (u_b, v_b)$ at the boundary points. If the body moves, *i.e.* $\mathbf{v} \neq 0$, then the position of the boundary points at each time step is computed by integration of $\mathbf{v} = \frac{d\mathbf{x}_s}{dt}$. The negative constants α and β are determined by observing the response of $\mathbf{U}$ once $\mathbf{F}$ is applied; α produces the natural oscillation frequency of the response, while β dampens the oscillation of the response. For unsteady flows, α must produce a response with a natural frequency greater than the highest frequencies present in the flow so that $\mathbf{F}$ can respond correctly to the changing flow field. The choice of α and β also influences the maximum time step allowable for each of the computations.

Goldstein *et al.* (1993) applied the forcing term only at points which coincided with the computational grid; in the current study, the boundary of the body is defined independent of the grid so that a smoother boundary is obtained. The effect of the virtual boundary points was then interpolated to the grid points via bilinear interpolation following Peskin (1972, 1982). Both Peskin (1972, 1982) and Goldstein *et al.* (1993) imposed the forcing term only at points which defined the boundary, thus allowing fluid motion inside the body. For Peskin's (1972, 1982) work this behavior is desirable since his calculations concern blood flow inside and outside of the heart. Goldstein *et al.* (1993) investigated the effect of solid bodies placed within a flow field which physically do not permit flow inside the boundary. Consequently, the flow fields which were numerically allowed to develop in such boundaries were unphysical and neglected by Goldstein *et al.* (1993). In the present

computations, very favorable results were obtained for some cases by imposing the forcing function not only on the boundary, but also *inside* the boundary of the body as well, depending on the conditions of the problem. For example, in the half-cylinder case where centerline symmetry is assumed (Fig. 4), imposition of the forcing function everywhere within the body yielded improved results. When the forcing was imposed only on the boundary, the internal flow field inside the body induced a small secondary vortex *outside* of the cylinder near the lower boundary which was independent of the main separation bubble. As a result, the length of the separation bubble was too long. This physical behavior was due to the shear free conditions imposed at the lower boundary of the computational domain interfering with the virtual boundary defining the cylinder. This condition was remedied by applying the forcing function everywhere within the cylinder. For the full cylinder simulations, the lower boundary did not interfere with the virtual boundary and very good results were obtained with the forcing function applied only at the boundary of the cylinder.

In an earlier work by the authors (Saiki & Biringen 1994), the virtual boundary technique was used in a different numerical algorithm which implemented Chebyshev polynomials in the wall-normal direction. As observed by Goldstein *et al.* (1993), due to the global nature of the Chebyshev polynomials, nongrowing, spatial oscillations in the normal and streamwise directions developed in the flow field when the feedback forcing function was applied, however, the oscillations did not appear to affect the flow field downstream of the body. In the present work, the application of the finite differences in the normal direction drastically reduced these spatial oscillations. The effect of these different discretization methods is illustrated in results obtained from computations of startup flow over a cylinder at $Re = 550$ (Figs. 1 and 2). Contours of streamwise velocity reveal the spatial oscillations which arise due to the Chebyshev discretization (Fig. 1a) and the attenuation of the oscillations with the application of finite differences (Fig. 1b). Comparison of the streamwise profiles in the normal direction (Fig. 2) provide clear evidence that the oscillations are strongly damped.

Results

Stationary cylinder in uniform flow

The cases investigating uniform flow over a stationary cylinder examined Reynolds numbers ($Re = \frac{U_\infty D}{\nu}$) ranging from $Re = 25$ to $Re = 400$. At $Re = 30$, we assumed centerline symmetry and considered the upper half of the cylinder, while for the other cases, $Re = 25$, 50, 65, 100, 200, and 400, the entire body of the cylinder was prescribed. The mesh resolution and computational domain dimensions are given in Table 1 for each case. For the symmetric case, the mesh was stretched only in the normal direction and for the full cylinder cases mesh stretching was employed in both directions with grid clustering near the body. As the Reynolds number increased, the length of the buffer domain at the outflow boundary was increased in order to accommodate the stronger vortices which were shed from the cylinder. The feedback forcing coefficients were set to $\alpha = -400000$ and $\beta = -600$, and the number of points defining the cylinder ranged from 1441 to 6900. The velocity components of the boundary points, **v**, were set to zero.

At low Reynolds numbers, ($4.5 \leq Re \leq 35$), experiments reveal an attached, steady, symmetric, recirculating bubble which develops downstream of the cylinder (Coutanceau & Defaye 1991). In the present simulations this behavior is clearly observed in the stream-function and spanwise vorticity contours for $Re = 25$ and $Re = 30$, respectively (Figs. 3 and 4). The physical parameters of the separation bubble are compared with previous experimental and computational studies in Table 2 and show good agreement for both Reynolds numbers.

As expected, when the Reynolds number was increased to $Re = 50$ the separation bubble became asymmetric (Fig. 5) and the two vortices in the bubble began to "pulse" with a distinct frequency which can be defined in terms of the Strouhal number, $St = \frac{U_\infty f}{D}$, where f is the dimensional frequency (Table 3). Furthermore, for this case the tail of the wake exhibited a "wavy" behavior. These results agree well with experimental observations in the $35 \leq Re \leq 60$ range, however, they are contrary to several computational results: at $Re = 50$, Gresho *et al.* (1984) observed vortex shedding from the cylinder and no attached separation bubble. It is interesting to note, however, that the Strouhal num-

bers for these simulations are very similar ($St = 0.135$ for the present and $St = 0.14$ for Gresho *et al.* 1984). In the computational studies of Jordan & Fromm (1972) and Braza *et al.* (1986), no vortex shedding or asymmetry of the separation bubble was observed for Reynolds numbers up to 1000. Braza *et al.* (1986) explained this behavior by stating that the computational scheme was too "clean," *i.e.* no external perturbations existed (as would appear in an experiment), therefore there was nothing to trigger any asymmetry or unsteadiness of the flow field. To induce the vortex shedding in their simulations the flow field was numerically perturbed. In the present work, as in the other related studies (Gresho *et al.* 1984; Karniadakis & Triantafyllou 1992; Engelman & Jaminia 1990), no such perturbation was needed to obtain unsteady flow.

According to experimental results, increasing the Reynolds number beyond $Re = 60$ leads to the development of a Kármán vortex street forced by vortices which are shed alternately with a distinct frequency from the top and bottom of the cylinder (Coutanceau & Defaye 1991). In the present study, the formation of the vortex street is depicted clearly in spanwise vorticity contours for $Re = 65$, 100, 200 and 400 (Figs. 6-9). In figure 10, vertical velocity contours for $Re = 400$ are plotted indicating a very smooth solution free of any detectable residual oscillations. As the Reynolds number increases, the frequency of the shedding increases (Table 3) and the vortices become more concentrated. The patterns obtained for $Re = 65$ and $Re = 100$ show remarkable similarity to the flow visualizations of Freymuth, Finaish, & Bank (1986). The time spectra and signature of the streamwise velocity at a point downstream of the cylinder reveals the presence of a spike at the vortex street Strouhal number; higher harmonics of the Strouhal number are also present (Fig. 11-14). Experiments predict that the onset of three-dimensionality and turbulence will occur at Reynolds numbers below $Re = 200$ (Coutanceau & Defaye 1991). Because of the two-dimensional nature of the current computations, turbulence and the effects of three-dimensionality cannot be obtained, however, the vortices shed from the cylinder at $Re = 200$ and 400 exhibit some irregularities associated with higher harmonics which subside as the vortices are convected downstream forming a laminar Kármán vortex street (Figs. 8 and 9).

Tables 3 and 4 summarize the drag coefficient (C_d), Strouhal number, the wavelength

of the Kármán vortex street (λ), and the vortex speed ($St\lambda$) observed for the unsteady solutions and provide comparisons with previous computational and experimental results. The Strouhal numbers obtained from the present results are slightly higher than the experimental results, however they correspond better than the values obtained by the majority of the other computational studies. The higher Strouhal number may be attributed to the size of the computational domain. Karniadakis & Triantafyllou (1992) found that if the inflow boundary was too close to the cylinder or if the domain was not wide enough, a higher Strouhal number was obtained. The distance between the inflow boundary and the cylinder in the current study ($L_i = 4$) is comparable to the domain length used by Gresho *et al.* (1984) and Engelman & Jaminia (1990), but shorter than those used by Karniadakis & Triantafyllou (1992), Braza *et al.* (1986), and Jordan & Fromm (1972). Accordingly, as shown in Table 4, the Strouhal number obtained in the current computations falls within the range of Strouhal numbers determined by the previous computational studies.

In the present study the drag coefficient was calculated in a manner similar to Goldstein *et al.* (1993); the drag was found by the considering the loss of fluid momentum in the domain, *i.e.*,

$$C_d = 2\int_{-\infty}^{\infty} \frac{U}{U_i}\left(1 - \frac{U}{U_i}\right)dy. \tag{2}$$

Due to the influence of the inflow boundary on the computation, U_i was defined as the velocity profile measured at a distance $\frac{D}{2}$ upstream of the cylinder. The influence of the inflow conditions on the drag coefficient has also been observed by Gresho *et al.* (1984). As Tables 3 and 4 reveal, good agreement is found for values of C_d in comparison with experiments and previous computational work.

Rotating cylinder in uniform flow

The startup flow over a cylinder rotating counter clockwise in uniform flow was computed for $Re = 200$. The rotation rate of the cylinder was $\omega = 1$, resulting in a tangential velocity of one half the freestream velocity ($v_t = 0.5$). The motion of the cylinder was introduced by setting the components of $\mathbf{v}$ in equation (1) to the proper streamwise and normal velocities arising from the rotation of the cylinder.

The characteristics of the startup flow at this Reynolds number and rotation rate con-

sist of a primary eddy evolving at the top of the cylinder and a developing second eddy below the x-axis of symmetry (Figs. 15a-15d). The second eddy moves upward (Figs. 15c-15d) inducing two secondary vortices which merge to form a single vortex at time, $t = 6$ (Figs. 15e-h). The streamfunction contours obtained by the current study (Fig. 15) are in remarkable agreement with experimental observations (Coutanceau & Ménard 1985) and previous computational results (Badr & Dennis 1985). Figure 16 demonstrates excellent comparison between profiles of streamwise and normal velocity along the x-axis behind the cylinder obtained from the current computation and experimental measurements (Coutanceau & Ménard 1985).

Oscillating cylinder in uniform flow

This computation was performed at $Re = 200$ with the cylinder oscillating parallel to the free-stream velocity at a frequency, $f_c = 1.88St$, *i.e.* 1.88 times the Strouhal frequency for the stationary cylinder. The amplitude of the oscillation resulted in a streamwise displacement of the cylinder of ± 0.24, and the cylinder motion was prescribed by setting the horizontal velocities on the boundary points to $u_b = A_c cos(2\pi f_c t)$. The computations started with the cylinder stationary and oscillations were imposed once the solution reached a quasi-steady state.

For the parameters considered in the current study, the vortex shedding pattern of the stationary case (Fig. 8) is modified by the oscillation of the cylinder as is clearly depicted in the time evolution of spanwise vorticity contours over two oscillation periods of the cylinder (Fig. 17). During this time period an antisymmetrical mode $A - III$ (Ongoren & Rockwell 1988) appears consisting of two clockwise vortices shed from the top of the cylinder and the evolution of a single counter clockwise eddy from the bottom. These vortices then form a vortex street with the weaker of the two clockwise vortices moving downstream alongside the counterclockwise eddy. These results are in excellent agreement with experimental observations (Griffin & Ramberg 1976; Ongoren & Rockwell 1988).

Conclusion

In this study, we applied a virtual boundary method to several steady/unsteady flow problems. The method models a no-slip boundary by an external forcing function added

to the momentum equations. The computational results for both stationary and moving cylinders in uniform flow compare favorably with both experimental and previous computational studies and lend further evidence to the applicability of the virtual boundary technique for steady and unsteady flow problems. The oscillations caused by the virtual boundary method when used with a spectral discretization method were attenuated by the application of high-order finite differences.

References

Badr, H. M. & Dennis, S. C. R. 1985 Time-dependent viscous flow past an impulsively started rotating and translating circular cylinder. *J. Fluid Mech.* **158**, 447.

Berger, E. & Wille, R. 1972 Periodic flow phenomena. *Ann. Rev. Fluid Mech.* **4**, 313.

Braza, M., Chassaing, P., & Minh, H. Ha 1986 Numerical study and physical analysis of the pressure and velocity fields in the near wake of a circular cylinder. *J. Fluid Mech.* **165**, 79.

Clift, R., Grace, J. R., & Weber, M. E. 1978 Bubbles, drops, and particles. Academic Press, New York.

Coutanceau, M. & Bouard, R. 1977 Experimental determination of the main features of the viscous flow in the wake of a circular cylinder in uniform translation. Part I. Steady flow. *J. Fluid Mech.* **79**, part 2, 231.

Coutanceau, M. & Ménard, C. 1985 Influence of rotation on the near-wake development behind an impulsively started cylinder. *J. Fluid Mech.* **158**, 399.

Coutanceau, M. & Defaye, J. R. 1991 Circular cylinder wake configurations: A flow visualization survey. *Appl. Mech. Rev.* **44**, 255.

Danabasoglu, G., Biringen, S., & Streett C. L. 1991 Spatial simulation of instability control by periodic suction blowing. *Phys. Fluids A* **3**, 2138.

Danabasoglu, G., 1992. Spatial simulation of transition in wall-bounded shear flows: Active control and effects of surface roughness. Ph.D. Thesis, University of Colorado.

Engelman, M. S. & Jaminia, M. 1990 Transient flow past a circular cylinder: A benchmark solution. *Int. J. Num. Meth. Fluids* **11**, 985.

Freymuth, P., Finaish, F., & Bank W. 1986 Visualization of the vortex street behind a circular cylinder at low Reynolds numbers. *Phys. Fluids* **29**, 1321.

Goldstein, D., Handler, R., & Sirovich, L. 1993 Modeling a no-slip boundary with an external force field. *J. Comp. Phys.* **105**, 354.

Gresho, P. M., Chan, R., Upson, C., & Lee, R. 1984 A modified finite element method for solving the time-dependent incompressible Navier-Stokes equations. Part 2. Applications. *Int. J. Numer. Meth. Fluids* **4**, 619.

Griffin, O. M. & Ramberg, S. E. 1976 Vortex shedding from a cylinder vibrating in line with an incident uniform flow. *J. Fluid Mech.* **75**, part 2, 31.

Huser, A. & Biringen, S. 1992 Calculation of two-dimensional shear-driven cavity flow at high Reynolds numbers. *Int. J. Num. Meth. in Fluids* **14**, 1087.

Jordan S. K. & Fromm, J. E. 1972 Oscillatory drag, lift, and torque on a circular cylinder in a uniform flow. *Phys. Fluids* **15**, 371.

Karniadakis, G. E. & Triantafyllou, G. S. 1992 Three-dimensional dynamics and transition to turbulence in the wake of bluff objects. *J. Fluid Mech.* **238**, 1.

Ongoren, A. & Rockwell, D. 1988 Flow structure from an oscillating cylinder. Part 2. Mode competition in the near wake. *J. Fluid Mech.* **191**, 225.

Peskin, C. S. 1972 Flow patterns around heart valves: A numerical method. *J. Comp. Phys.* **10**, 252.

Peskin, C. S. 1982. The fluid dynamics of heart valves: experimental, theoretical, and computational methods. *Ann. Rev. Fluid Mech.* **14**, 235.

Roshko, A. 1953 On the development of turbulent wakes from vortex streets. *NACA Technical Note* 2913.

Saiki, E. M., Biringen, S., Danabasoglu, G., & Streett, C. L. 1993 Spatial simulation of secondary instability in plane channel flow: Comparison between H- and K-type disturbances. *J. Fluid Mech.* **253**, 485.

Saiki, E. M. & Biringen, S. 1994 Numerical simulation of particle effects on boundary layer flow. To appear in *NASA/ICASE Transition, Turbulence, and Combustion Workshop Proceedings*, Springer-Verlag.

Streett, C. L. & Hussaini, M. Y. 1986 Finite length effects in Taylor-Couette flow. ICASE Report No. 86-59.

Streett, C. L. and Macaraeg, M. G., 1989. Spectral multi-domain for large-scale fluid dynamic simulations. *Appl. Num. Math* **6**, 123.

Re	$N_x x N_y$	$L_x x L_y$	Δx_{min}	Δy_{min}
25	267x147	20x10	0.0375	-.0375
30	481x71	7x2	0.0125	0.001
50	267x147	20x10	0.0375	0.0375
65	363x147	28x10	0.0375	0.0375
100	363x147	28x10	0.0375	0.0375
200	436x147	34x10	0.0375	0.0375
400	387x147	30x10	0.0375	0.0375

Table 1: Mesh resolution and computational domain dimensions (buffer domain is not included).

Properties of the wake behind a stationary cylinder	Re=25				Re=30	
	Present results	Gresho *et al.* (1984)*	Coutanceau & Bouard (1977)†	Cliff *et al.* (1978)†	Present results	Coutanceau & Bouard (1977)†
length of the separation bubble (L)	1.36	1.15	1.22	-	1.525	1.53
x-coordinate of the center of the vortex cores (a)	0.53	0.38	0.44	-	0.55	0.55
y-distance between the vortex cores (b)	0.5	0.47	0.51	-	0.494	0.54
minimum streamwise velocity on the axis of symmetry (u_{max})	-0.064	-0.057	-0.057	-	-0.1052	-0.0743
x-coordinate of minimum streamwise velocity on the axis of symmetry (d)	0.59	0.49	0.5	-	0.625	0.64
separation angle (θ)	45°	45°	48°	-	49°	50.1°
drag coefficient (C_d)	1.54	2.26	-	1.84	-	-

*. computational study
†. experiment

Table 2: Comparison of the wake properties behind a stationary cylinder with experiments and previous computational results for Re=25 and Re=30; steady flow solutions.

Re	Drag coefficient: C_d*			Strouhal number: St				Wavelength: λ		Vortex speed: Stλ	
	Present results	Gresho *et al.* (1984)†	Cliff *et al.* (1978)‡	Present results	Gresho *et al.* (1984)†	Roshko (1953)‡	Berger & Wille (1972)‡	Present results	Gresho *et al.* (1984)†	Present results	Gresho *et al.* (1984)†
50	1.4	1.81	1.41	0.135	0.14	0.122	0.12-0.13	-	6.5	-	0.93
65	1.33	-	1.33	0.152	-	0.143	-	5.9	-	0.8968	-
100	1.26	1.76	1.24	0.171	0.18	0.167	0.16-0.17	5.5	5.2	0.9405	0.93
200	1.18	1.76	1.16	0.197	0.21	-	0.18-0.19	4.8	4.4	0.9456	0.92
400	1.18	1.78	1.12	0.22	0.22	0.205	0.2-0.21	4.4	4.4	0.968	0.96

*. Drag coefficient is averaged in the unsteady cases.
†. computational study
‡. experiment

Table 3: Comparison of quantitative data with results from experiments and previous computational studies; unsteady flow solutions.

Re=100	Present results	Gresho *et al.* (1984)	Engelman & Jaminia (1990)	Braza *et al.* (1986)	Jordan & Fromm (1972)	Karniadakis *et al.* (1992)
C_d	1.26	1.76	1.411	1.28	1.28	-
St	0.171	0.18	0.173	0.16	0.16	0.168
λ	5.5	5.2	5.32	-	-	-
$St\lambda$	0.9405	0.93	0.915	-	-	-

Table 4: Comparison of quantitative data with previous computational results for Re=100; unsteady flow solutions.

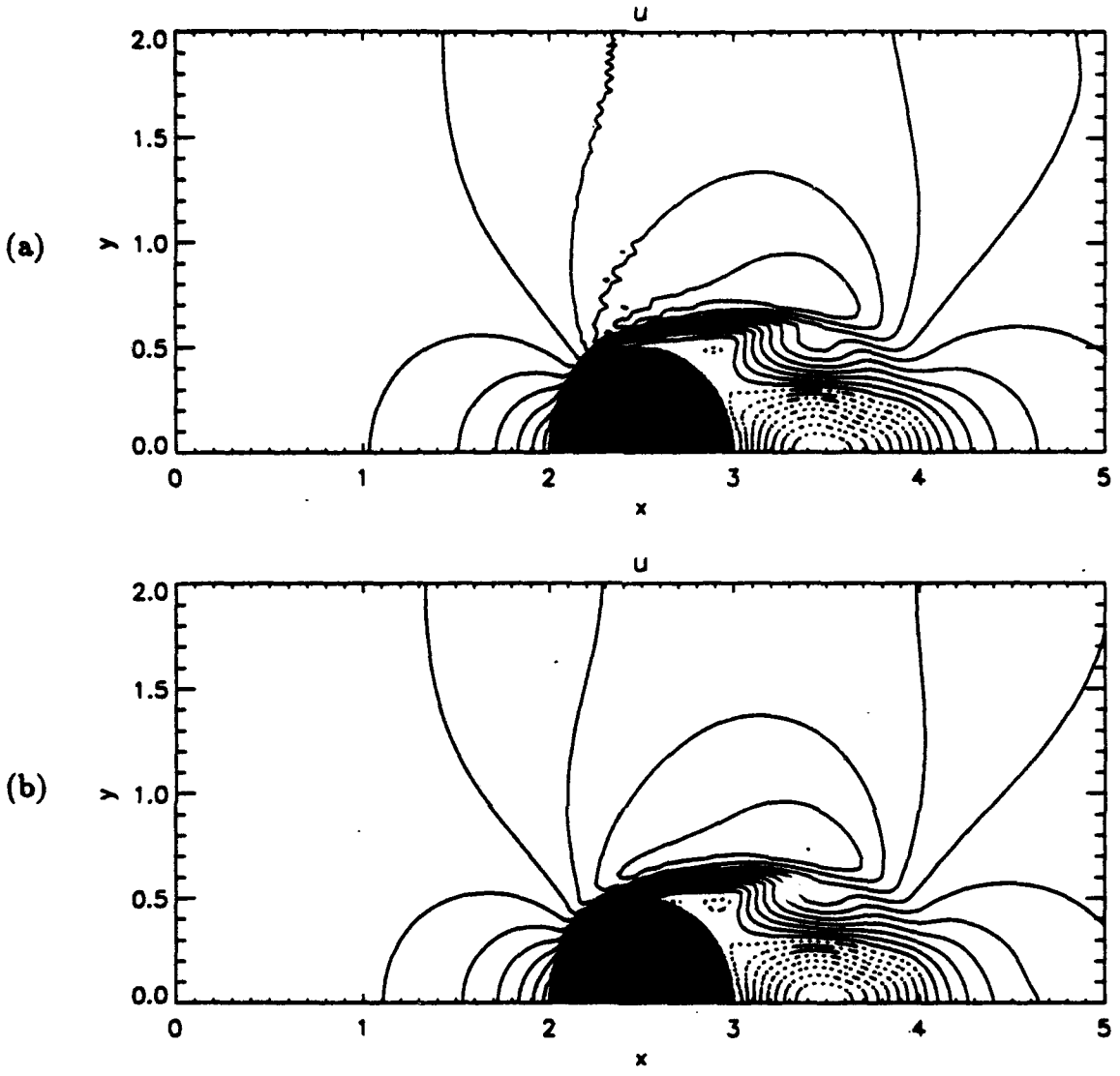

Figure 1. Re=550, $t = 3.0$: streamwise velocity, (a) Chebyshev; (b) finite differences.

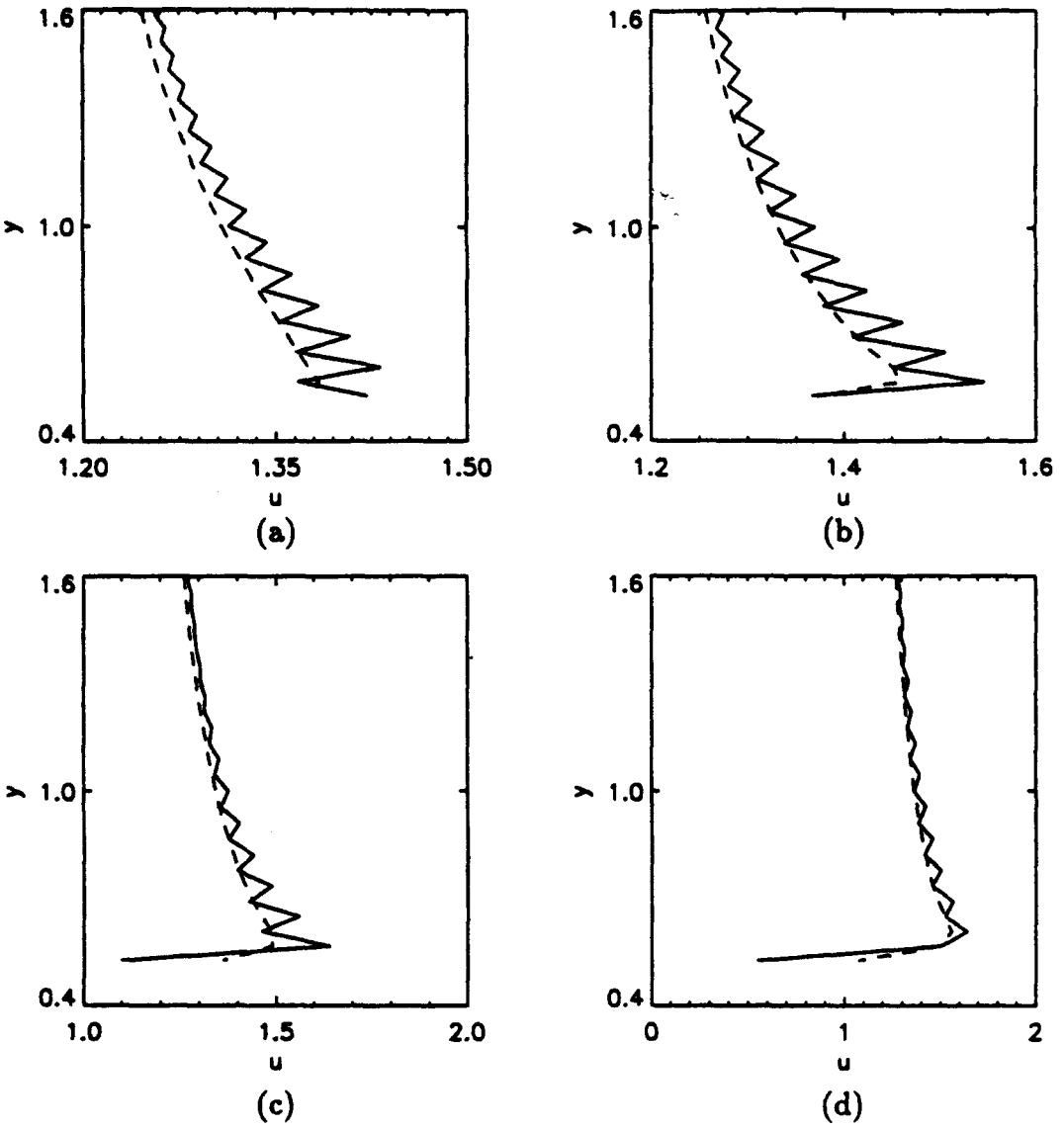

Figure 2. Re=550; normal profiles of streamwise velocity in the vicinity of the cylinder, (a) $x = 2.23750$; (b) $x = 2.2875$; (c) $x = 2.3125$; (d) $x = 2.3650$. ——— Chebyshev; – – – finite differences.

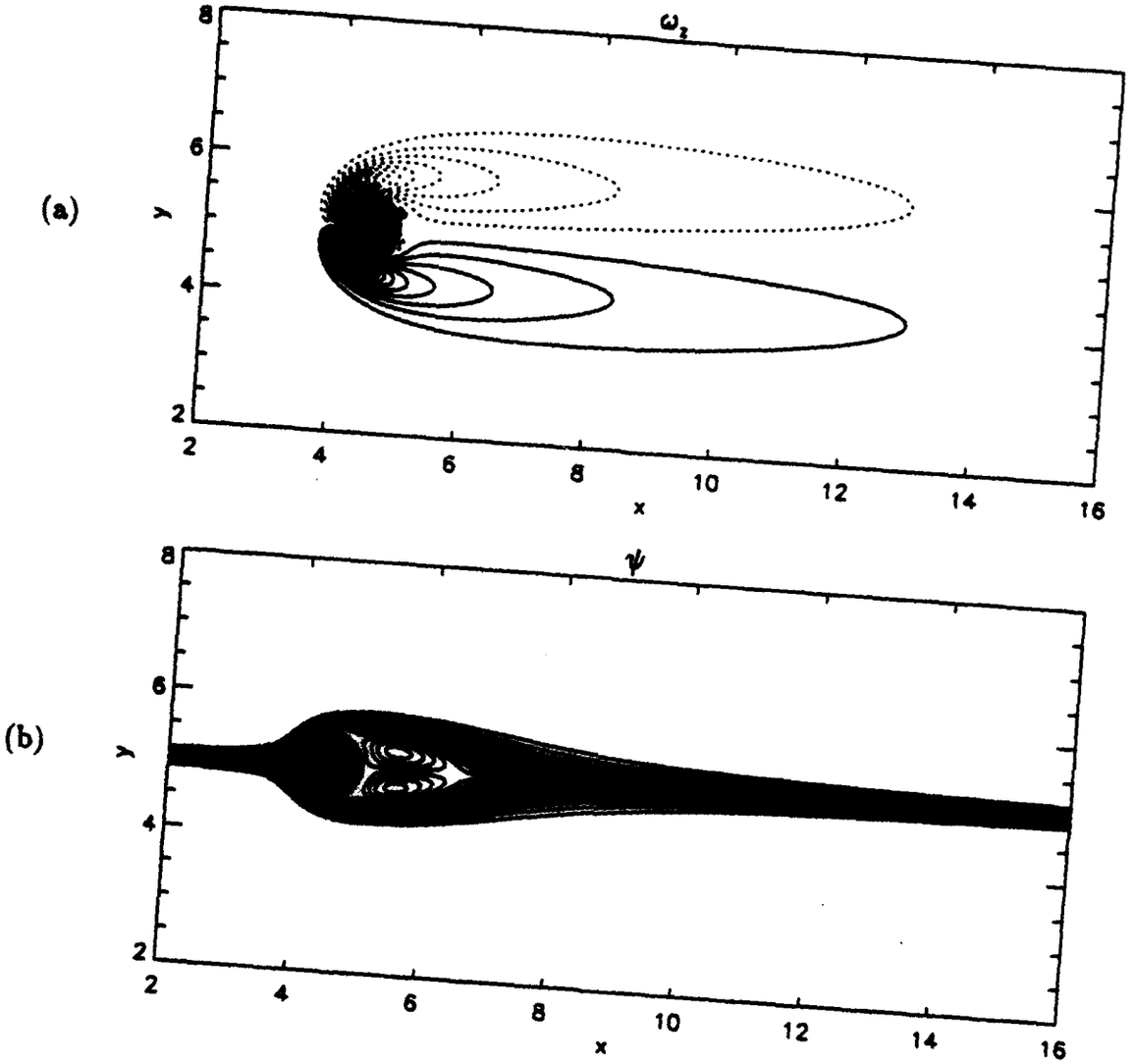

Figure 3. Re=25: (a) spanwise vorticity; (b) streamfunction.

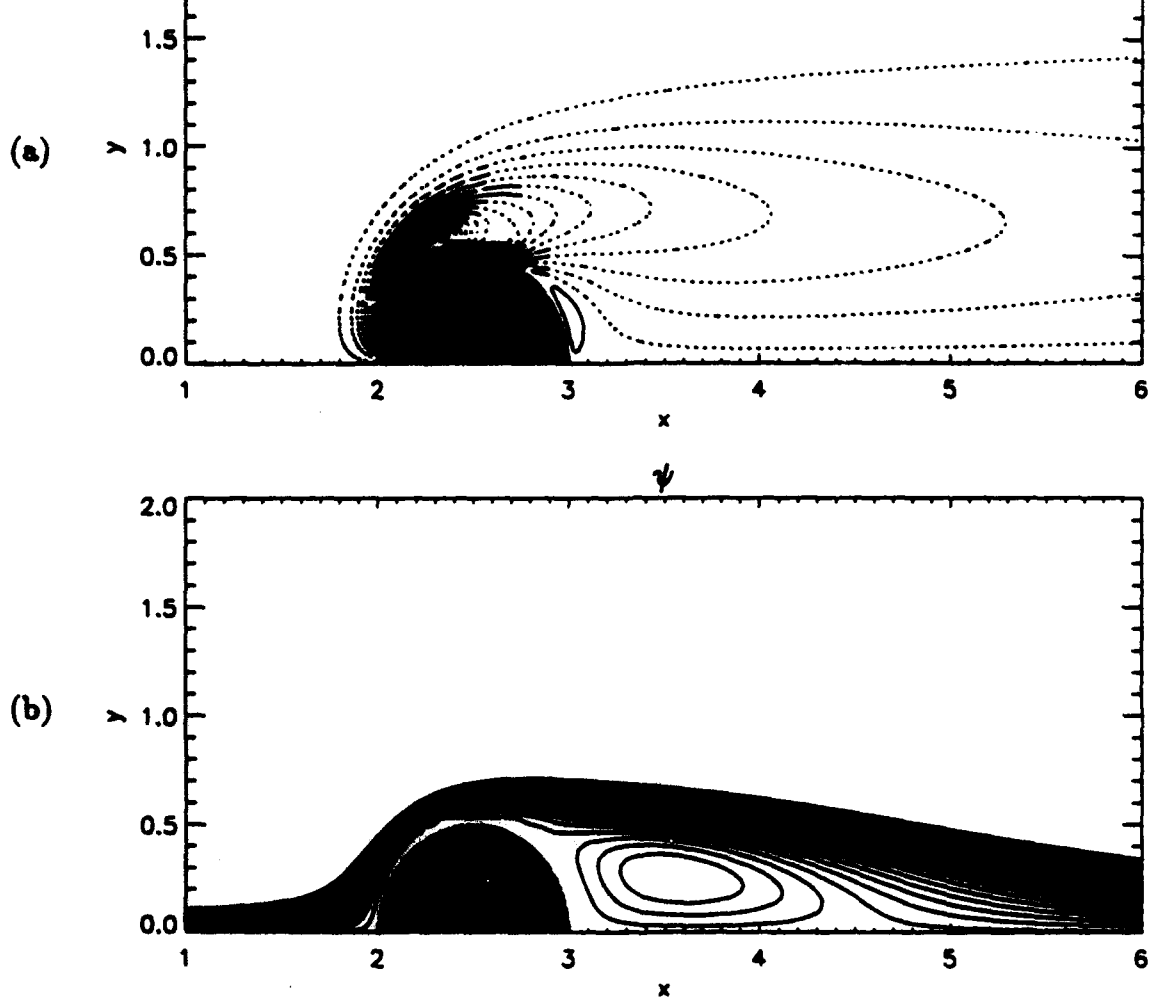

Figure 4. Re=30: (a) spanwise vorticity; (b) streamfunction.

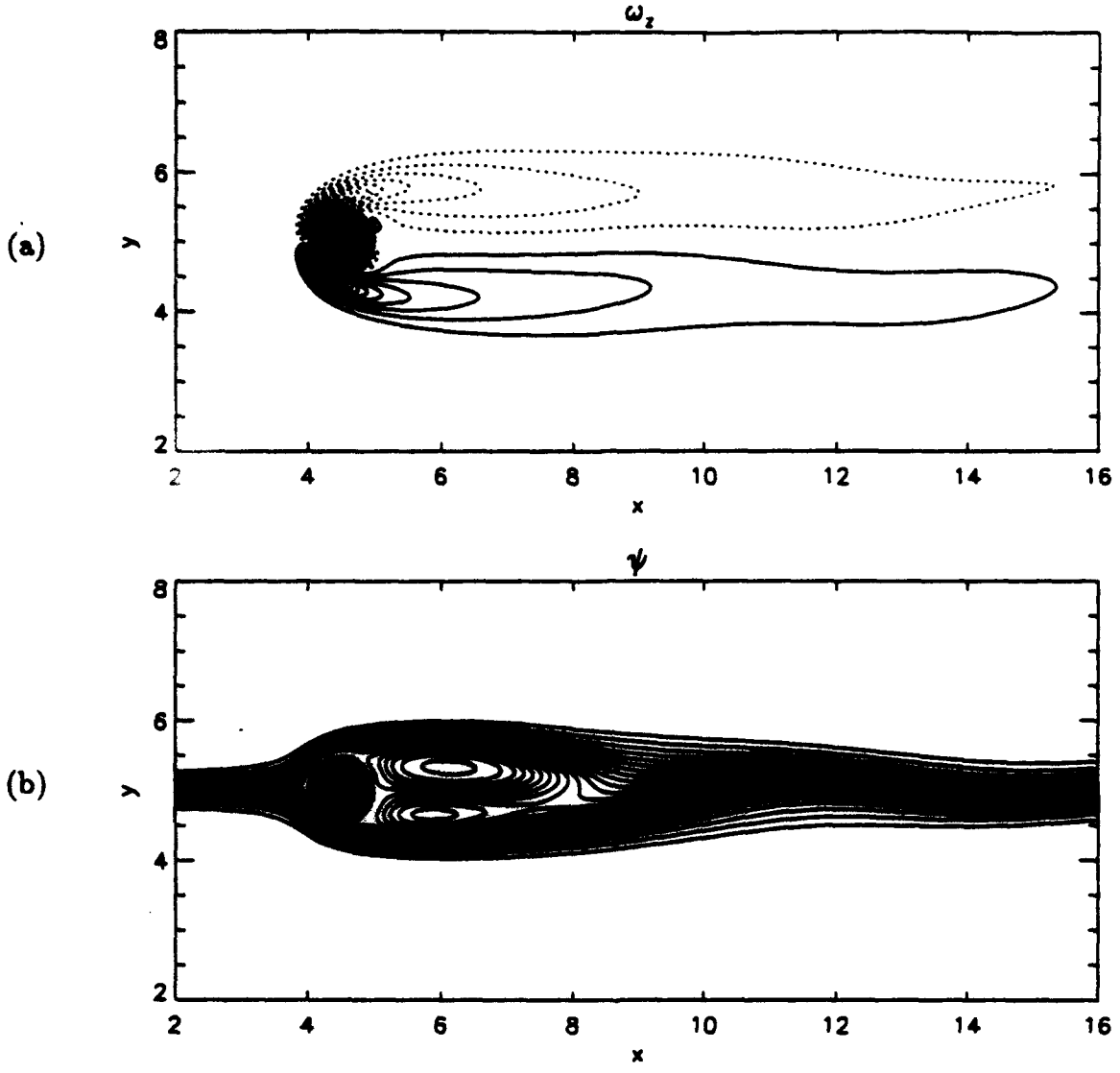

Figure 5. Re=50: Instantaneous snapshot of (a) spanwise vorticity; (b) streamfunction.

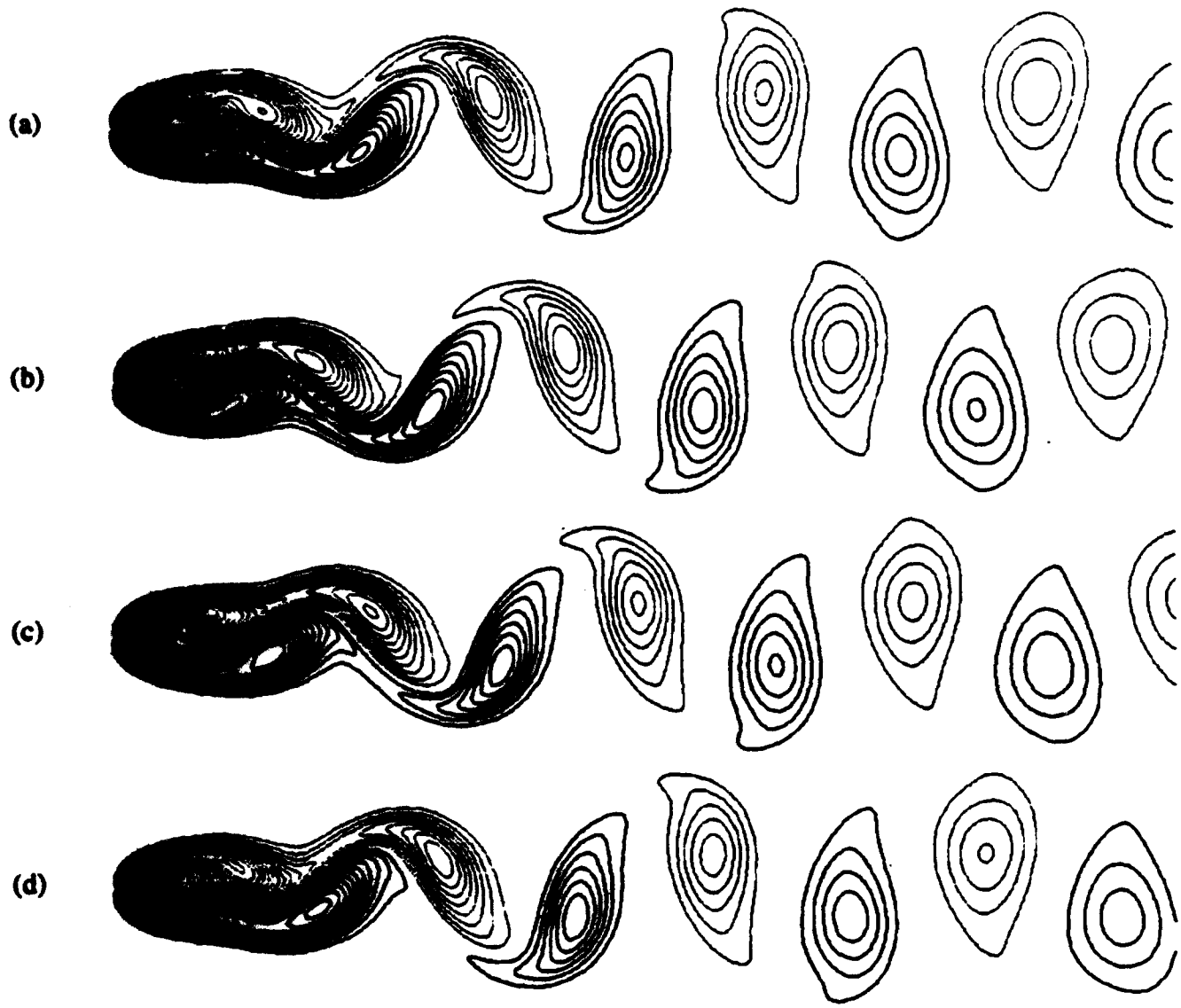

Figure 4. Re=65: Contours of spanwise vorticity. (a) t=0; (b) t=τ/4; (c) t=τ/2; (d) t=3τ/4 (τ=1/St).

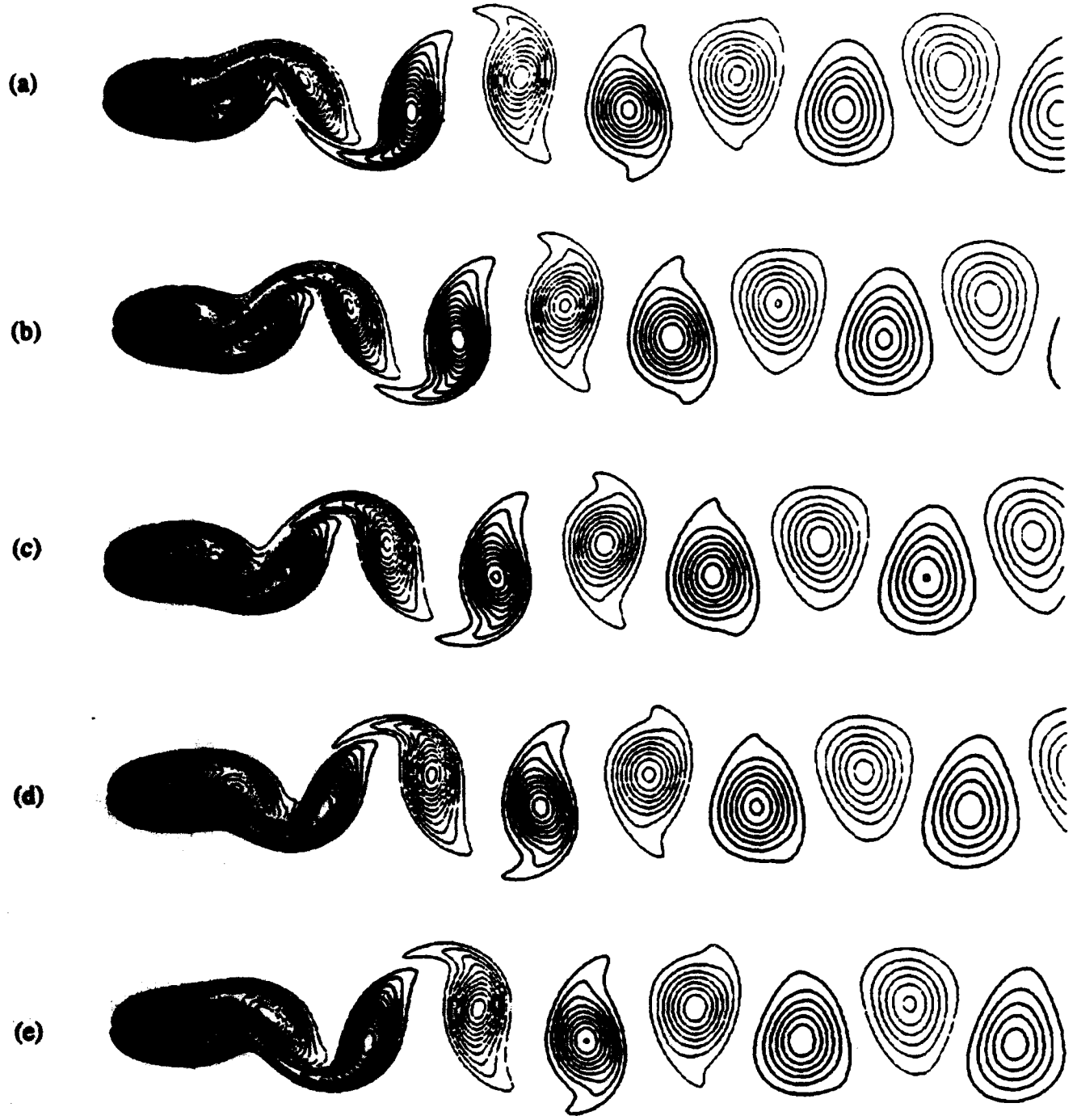

Figure 5. Re=100: Contours of spanwise voriticity. (a) t=0; (b) t=τ/5; (c) t=2τ/5; (d) t=3τ/5; (e) t=4τ/5 (τ=1/St).

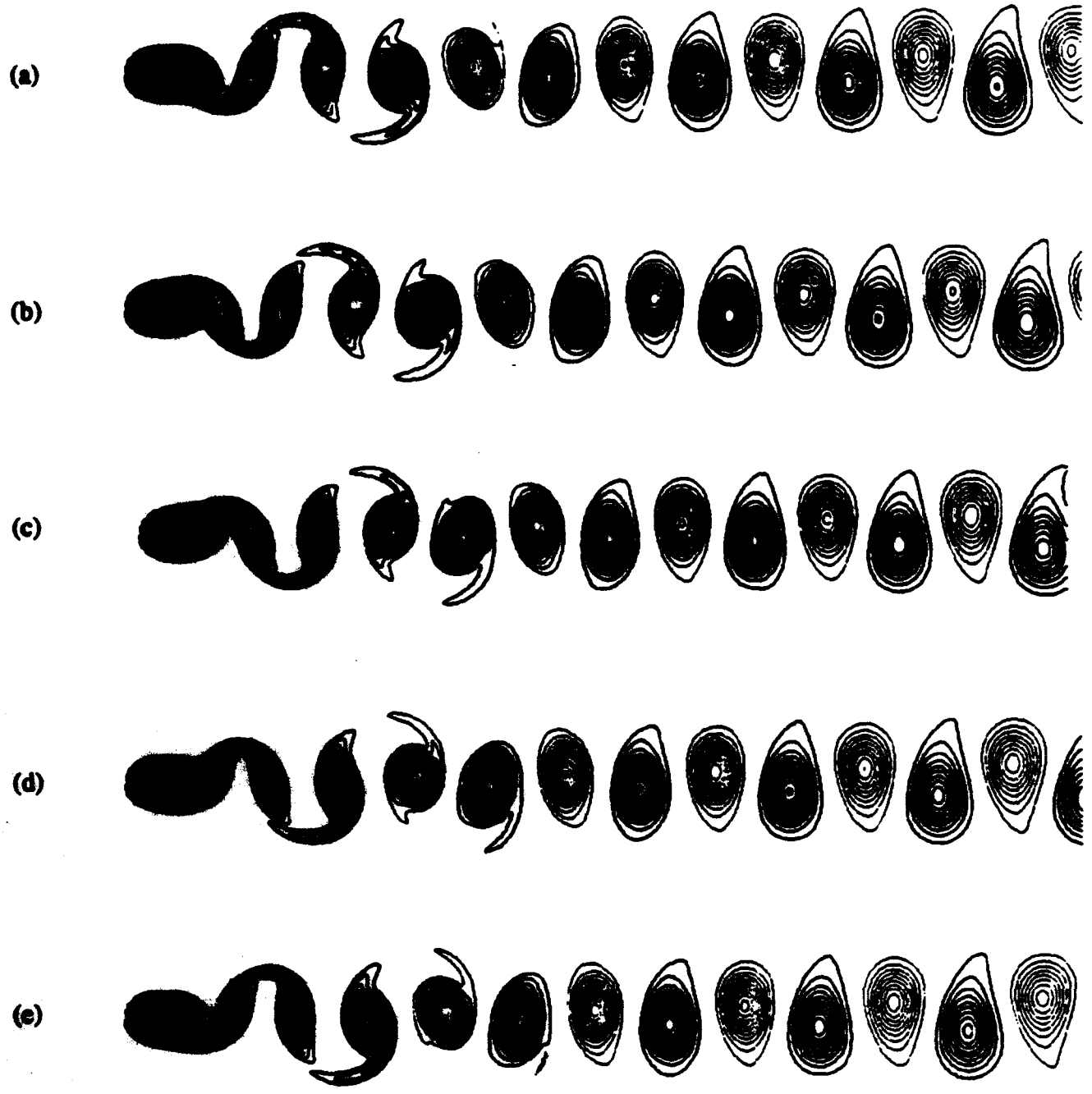

Figure 6. Re=200: Contours of spanwise vorticity. (a) t=0; (b) t=τ/5; (c) t=2τ/5; (d) 3τ/5; (e)4τ/5 (τ=1/St).

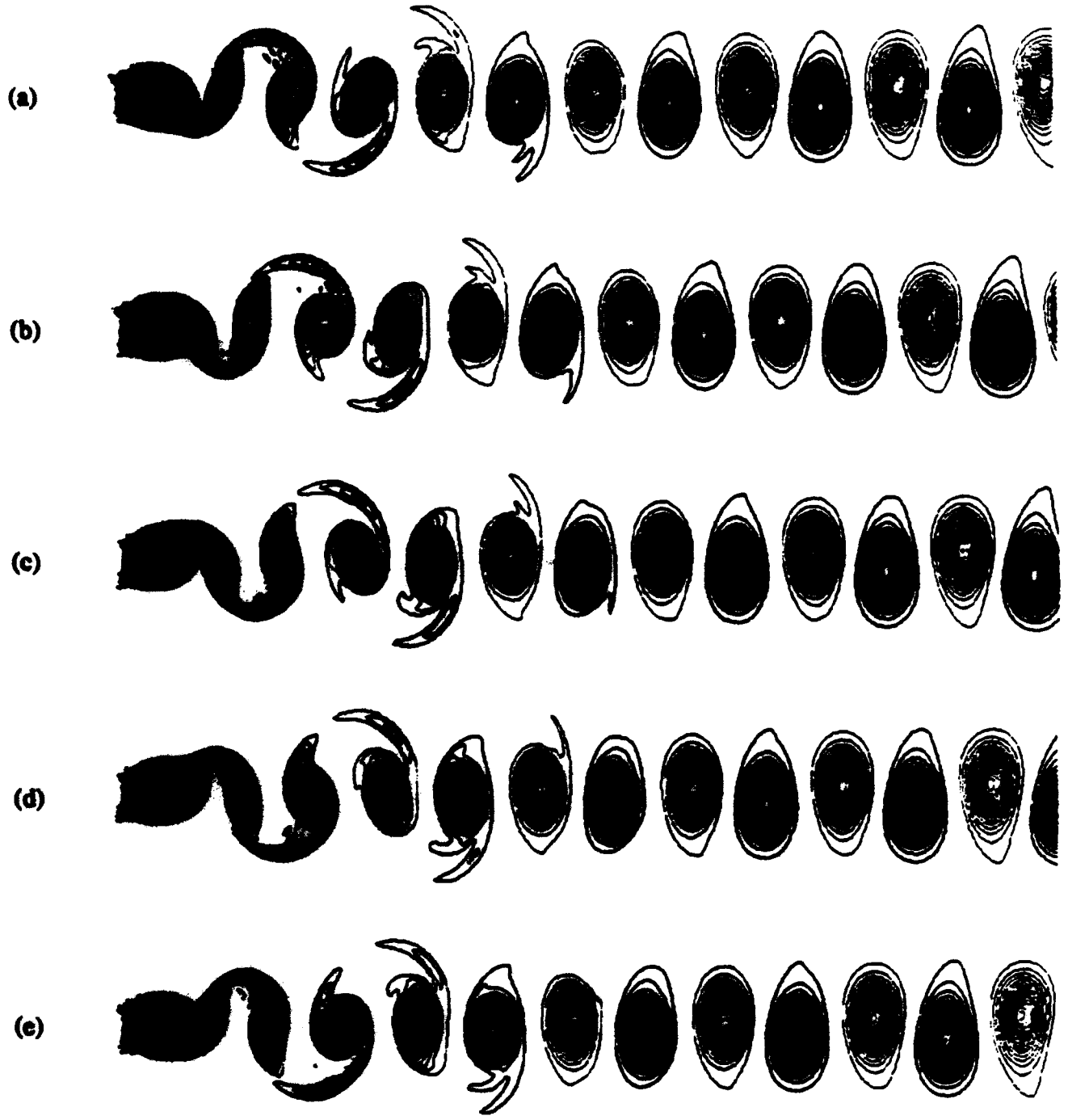

Figure 7. Re=400: Contours of spanwise vorticity. (a) t=0; (b) t=τ/5; (c) t=2τ/5; (d) t=3τ/5; (e) t=4τ/5 (τ=1/St).

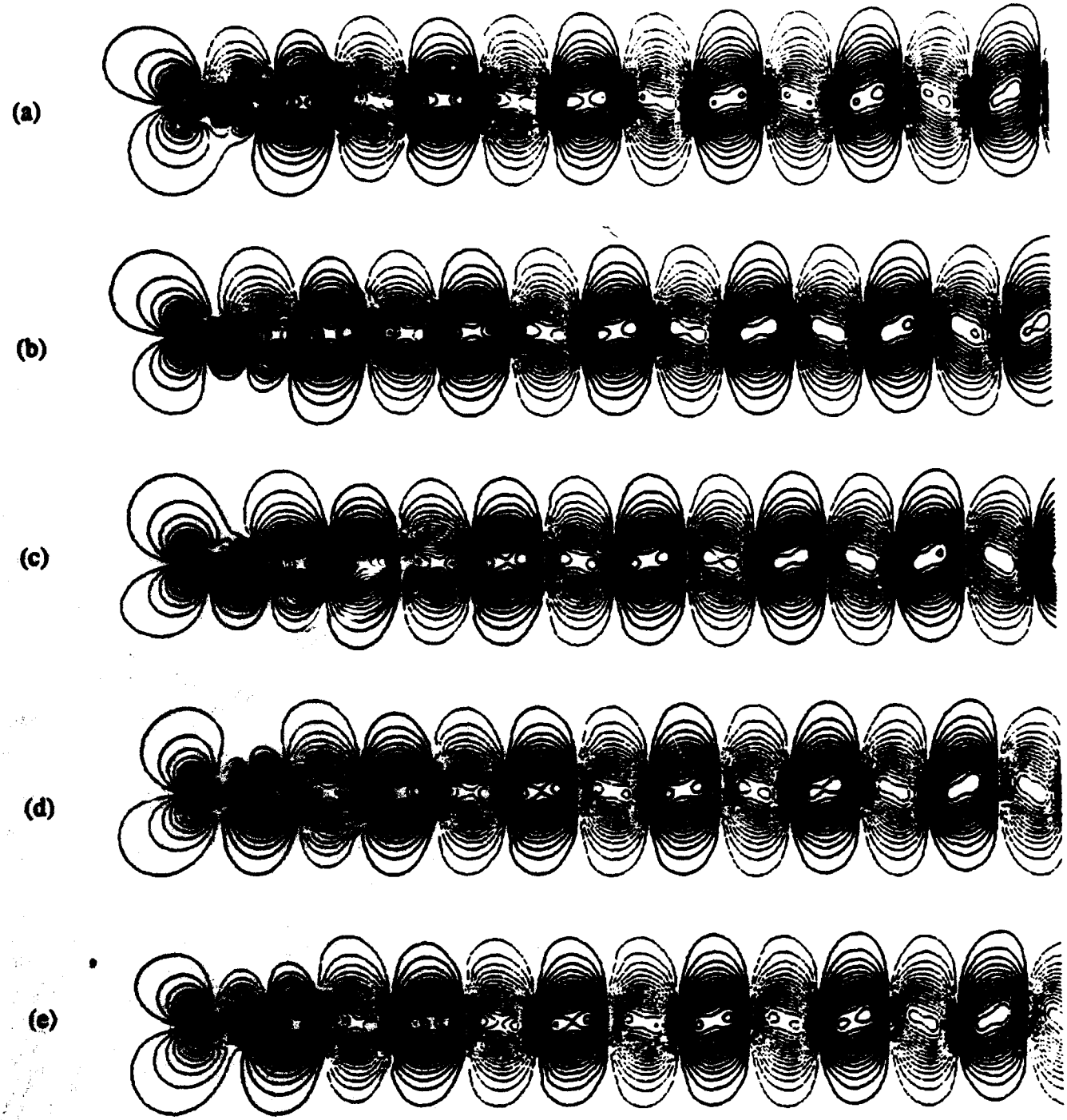

Figure 8. Re=400: Contours of normal velocity. (a) t=0; (b) t=τ/5; (c) t=2τ/5; (d) t=3τ/5; (e) t=4τ/5 (τ=1/St).

THIS PAGE IS MISSING IN ORIGINAL DOCUMENT

Figures 9 + 10

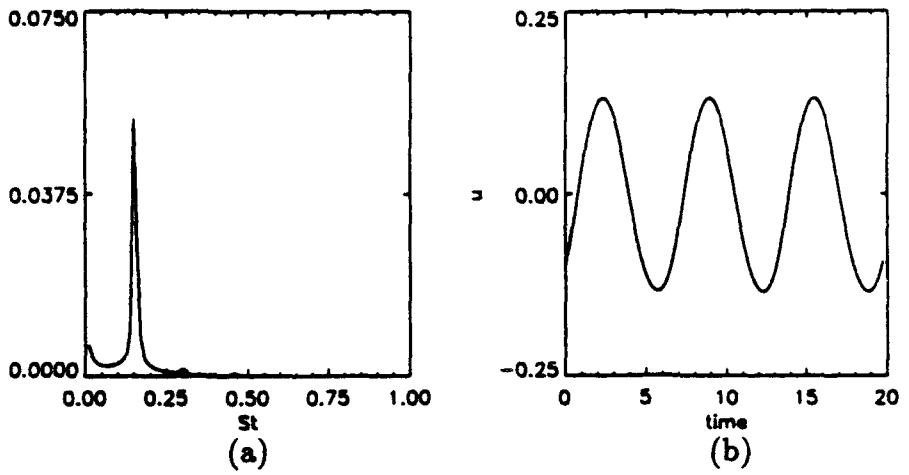

Figure 11. Re=65: (a) spectrum and (b) time signature of streamwise velocity measured at ($x_d = 0.9445$, $y_d = -0.325$); x_d is the streamwise distance downstream from the cylinder and y_d is the normal distance from the symmetry axis of the cylinder.

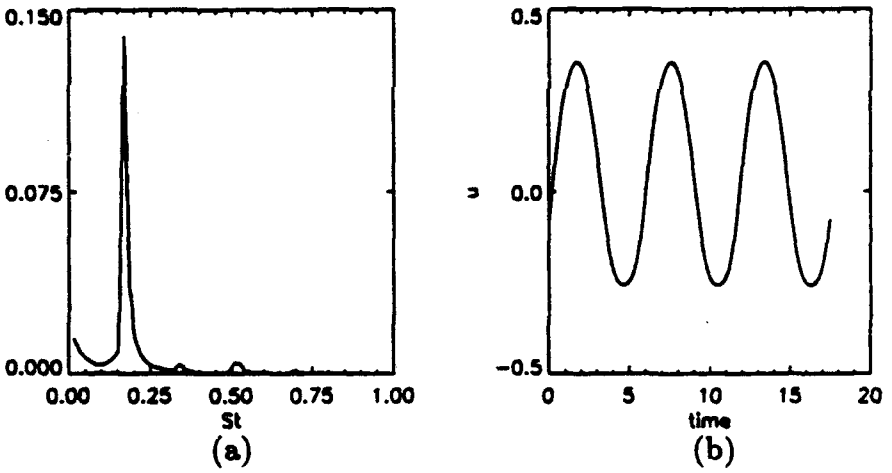

Figure 12. Re=100: same as Figure 11.

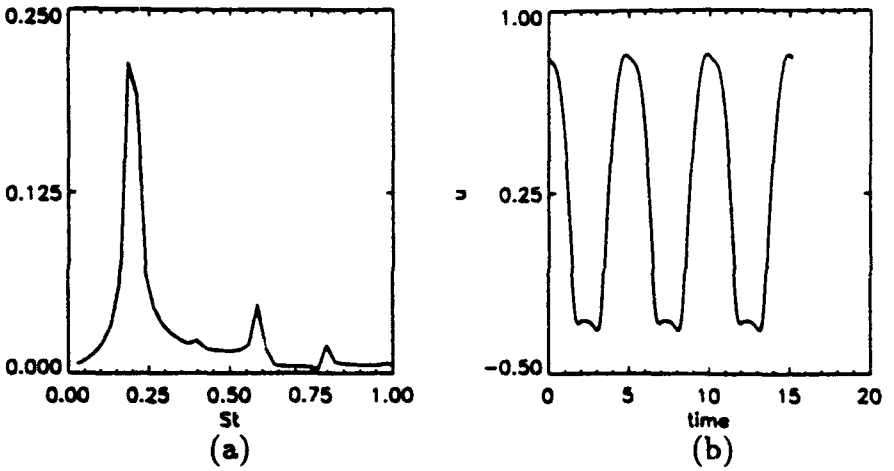

Figure 13. Re=200: same as Figure 11.

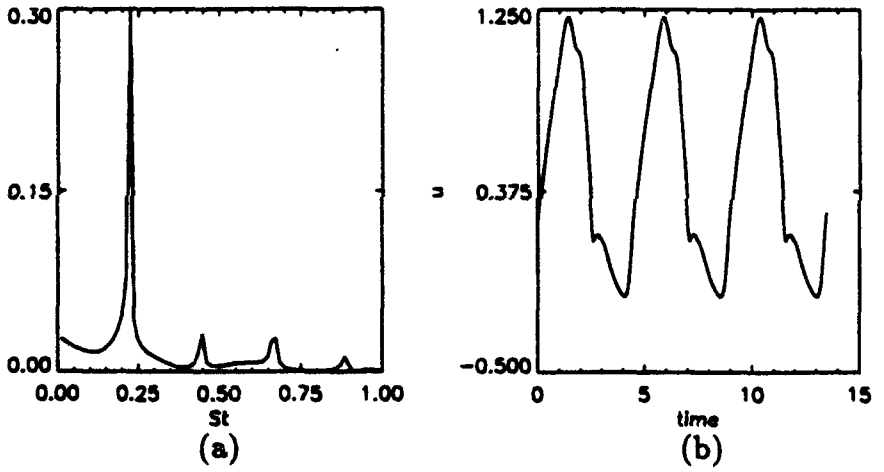

Figure 14. Re=400: same as Figure 11.

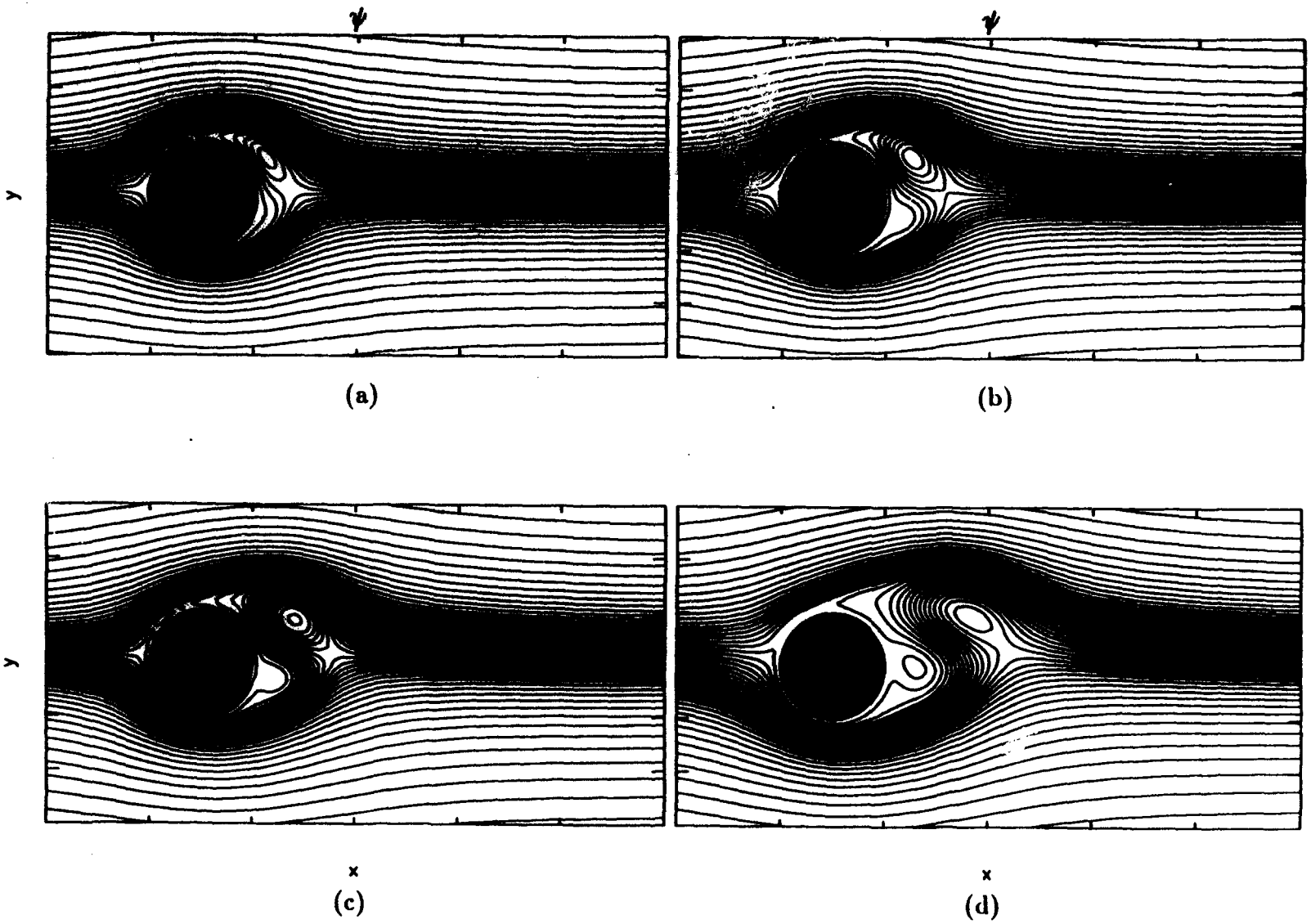

Figure 15. Re=200: Rotating cylinder. Time evolution of streamfunction contours. (a) $t = 1$; (b) $t = 1.5$; (c) $t = 2$; (d) $t = 3$; (e) $t = 4$; (f) $t = 5$; (g) $t = 5.5$; (h) $t = 6$.

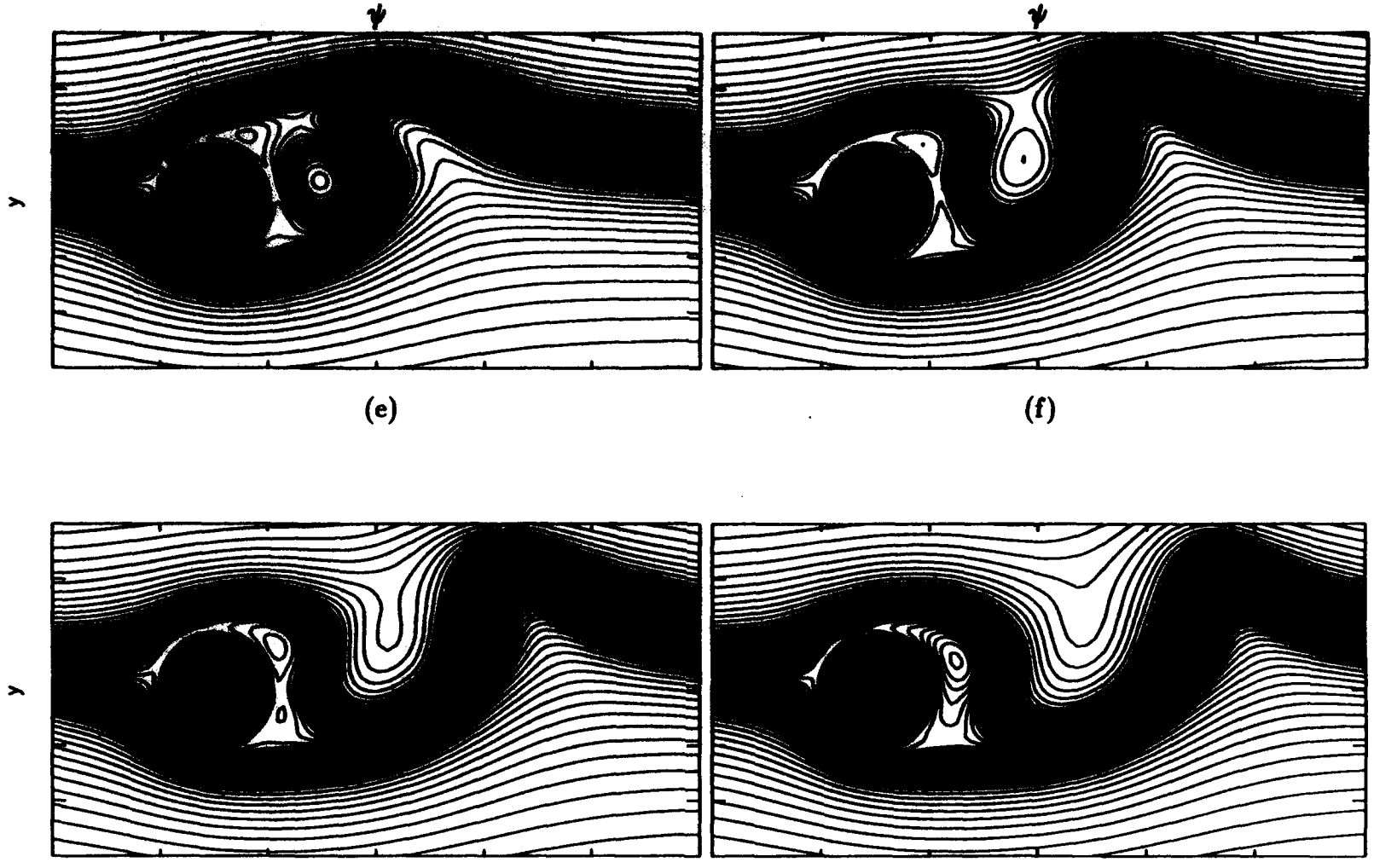

(e) (f)

(g) (h)

Figure 15. (cont)

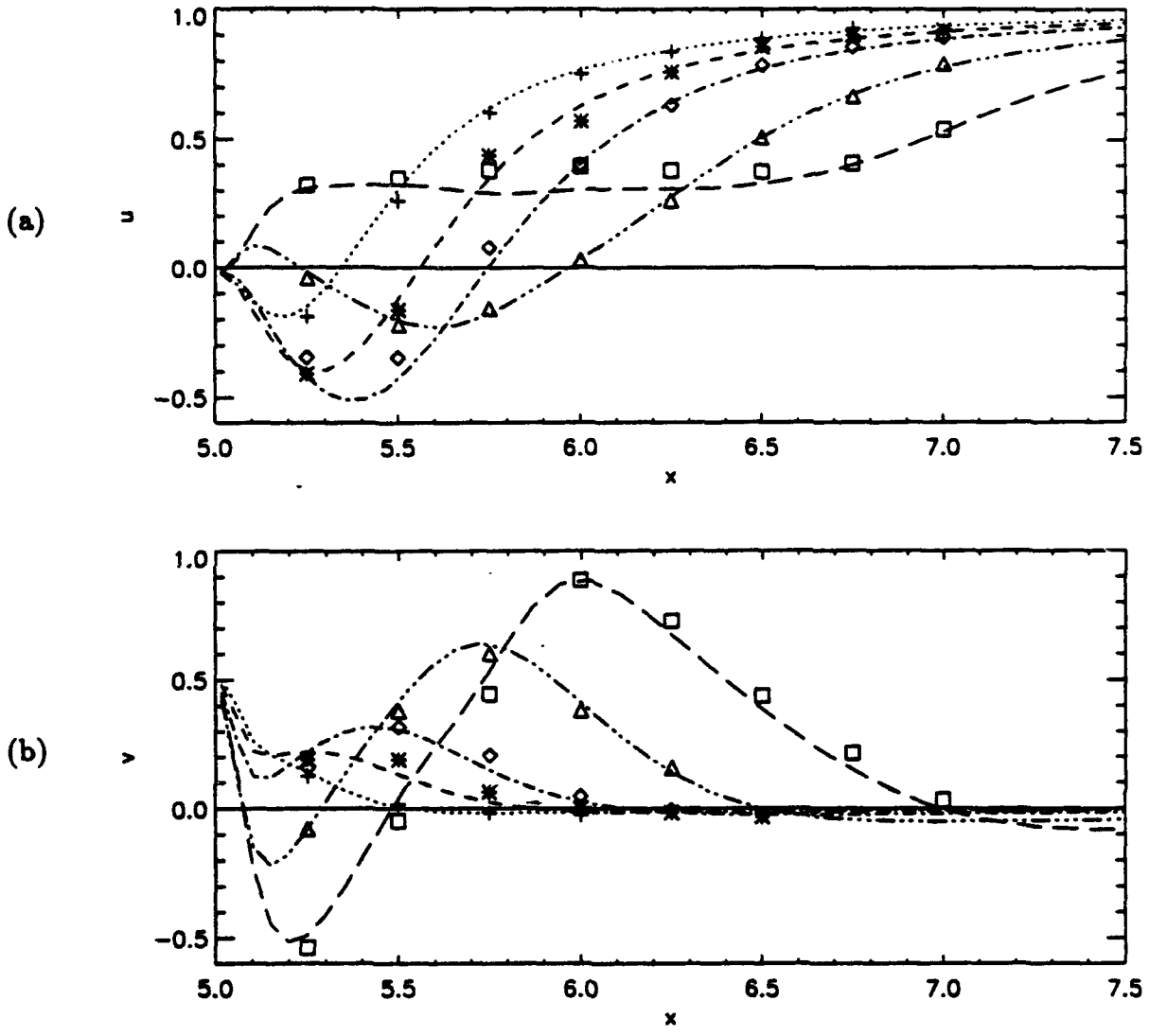

Figure 16. Re=200: Rotating cylinder. Time evolution of the velocity profiles along the x-axis; (a) streamwise velocity (b) normal velocity. Current computational results: ·····, $t = 1$; − − −, $t = 1.5$; −·−·−, $t = 2$; ·····, $t = 3$; — —, $t = 4$. Experimental results (Coutanceau & Ménard 1985): +, $t = 1$; ∗, $t = 1.5$; ◇, $t = 2$; △, $t = 3$; □, $t = 4$.

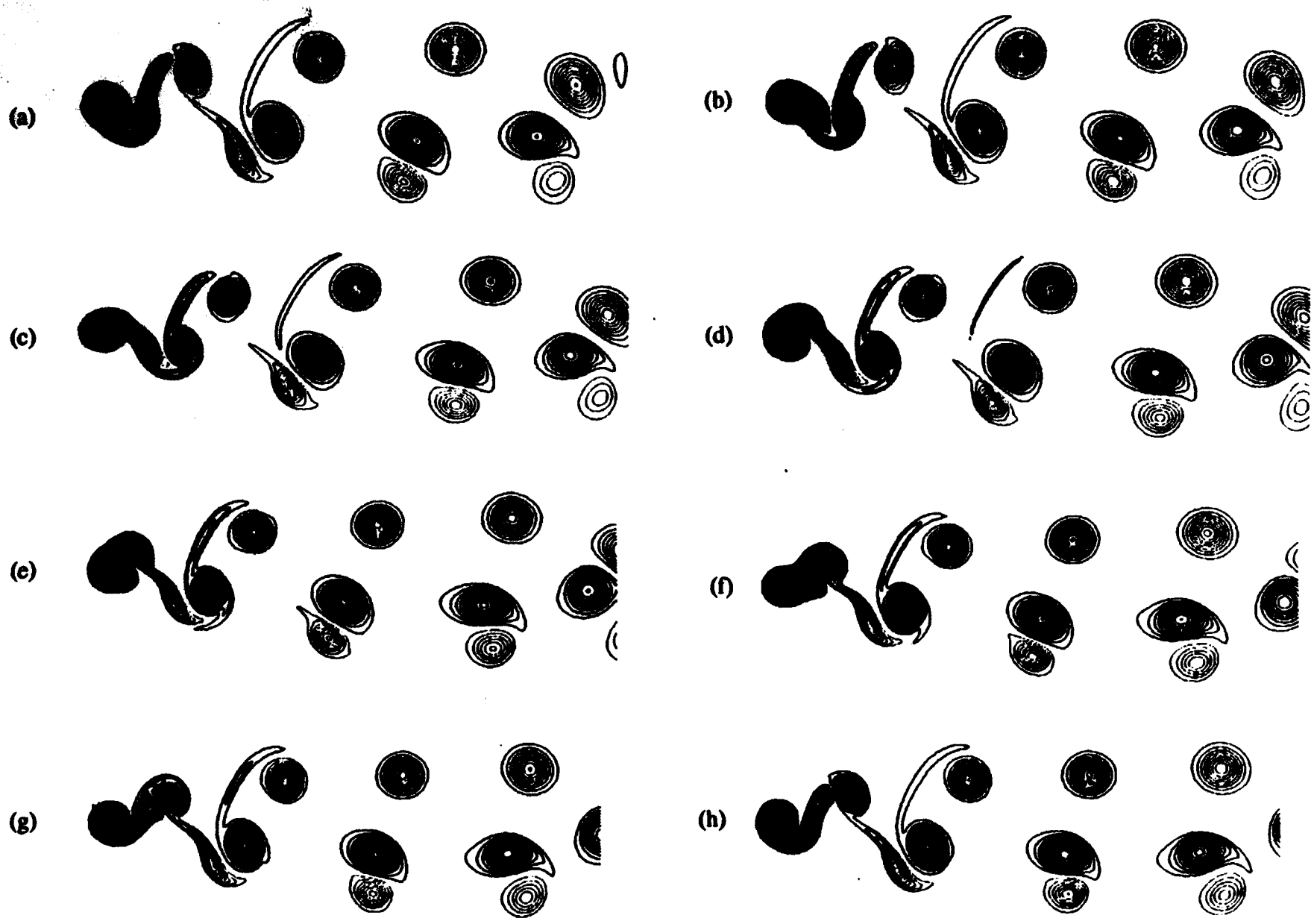

Figure 17. Re=200: Oscillating cylinder. Time evolution of spanwise vorticity contours; (a) t=T/4; (b) t=T/2; (c) t=3T/4; (d) t=T; (e) t=5T/4; (f) 3T/2 (g) 7T/4; (h) 2T (T = oscillation period of the cylinder).